ACS AGRICULTURAL SCIENCE & TECHNOLOGY

Open Access

This article is licensed under CC-BY 4.0

pubs.acs.org/acsagscitech

Article

Design and Performance of a Multicomponent Glass Fertilizer for Nutrient Delivery in Precision Agriculture

José Hermeson da Silva Soares, Thomaz William Boaventura, Ana Caroline A. de Moura, Letícia Cristina da Silva, Amauri Garcia Filho, Raiza L. Landgraf, Dânia Elisa Christofoletti Mazzeo, Alberto C. de Campos Bernardi, Ana Rita A. Nogueira, Eduardo B. Ferreira,* and Danilo Manzani*

Cite This: *ACS Agric. Sci. Technol.* 2025, 5, 142−157

Read Online

ACCESS | Metrics & More | Article Recommendations | Supporting Information

ABSTRACT: Glass fertilizers (GF) appear promising for use in agriculture since they can be "constructed" according to the demands of crops in the necessary quantities of macro and micronutrients in a single product. In the design of a GF, the different growth stages of a crop can be contemplated by considering the soil pH, irrigation regime, and composition. In this study, a multicomponent oxide glass is formulated for the nutritional Palisade grass (cv Piatã), used as a model for nutrients released in greenhouse experiments. The GF composition, which included P_2O_5−SiO_2−B_2O_3−CaO−K_2O−MgO−MnO_2−MoO_3−ZnO, was melted, cooled into a glass, and comminuted into grains with a particle size distribution between 0.85 and 2.0 mm in diameter. The GF solubility was previously evaluated through immersion in deionized water and citric acid-sodium citrate buffer solutions at different pH levels at 25 °C for 64 h. The undissolved glass fractions were analyzed using X-ray fluorescence (XRF), scanning electron microscopy (SEM), differential scanning calorimetry (DSC), infrared spectroscopy (FTIR), and Raman. The nutrient release rates, solubility, and results from five sequential harvests of Palisade grass were analyzed using inductively coupled plasma optical emission spectrometry (ICP-OES). The previous study reveals a slow release of nutrients through two dissolution mechanisms, ion exchange and hydrolysis reactions. Greenhouse experiments showcased the gradual release of nutrients and highlighted GF's efficiency in providing a continuous nutrient supply from a single fertilization. Compared with experiments using soluble salts in the same amount of the GF, it consistently produced a higher dry matter yield (DMY) than the control. It was observed that yields for five cuts presented approximately 70% greater agronomic efficiency for the experiment with GF. Standard ecotoxicological tests were also conducted. It was performed with *Allium cepa* and *Lactuca sativa*, and no genotoxic or phytotoxic effects were observed for the various concentrations and sizes of particles employed. These results represented a significant stride toward developing environmentally friendly glass fertilizers for prolonged nutrient release and tuned for precision farming.

KEYWORDS: *glass fertilizer, controlled dissolution rates, nutrient release mechanisms, multicomponent oxide glass, precision agriculture, ecotoxicological assays*

Downloaded via UNIV OF SAO PAULO on September 14, 2025 at 01:24:10 (UTC).
See https://pubs.acs.org/sharingguidelines for options on how to legitimately share published articles.

1. INTRODUCTION

The Brazilian Censo Agro 2017 reported a substantial 13.6% decline in pasture areas between 1995 and 2017, driven by fertile land degradation, reflecting a disproportionate relationship with livestock growth. Contributing factors include pest and disease outbreaks, inadequate forage plant management, and soil infertility.[1,2] Restoring degraded pastures to economically sustainable levels largely rely on addressing soil fertility issues.

Natural or synthetic fertilizers are essential for supplying nutrients to plants. They are indispensable for enriching the soil with elements for the plants' metabolism, boosting crop quality and productivity. For most crops, essential nutrients include hydrogen, oxygen, nitrogen, phosphorus, potassium, iron, manganese, zinc, copper, boron, chlorine, molybdenum, carbon, sulfur, magnesium, and calcium. These elements are crucial for physiological processes such as photosynthesis and respiration and are essential for synthesizing key biomolecules including nucleic acids, enzymes, and nucleotides. They also significantly affect transpiration, stomatal conductance, water use efficiency, and metabolite transport.[3,4]

Despite widespread use of NPK formulations, composed primarily of nitrogen, phosphorus, and potassium,[5] their efficiency is often limited by nutrient losses through fixation, leaching, and gaseous emissions shortly after application. This leads to frequent and excessive reapplications and environmental issues, such as surface and groundwater contamination, soil acidification or alkalization, and reduced soil fertility.[6] Studies have shown that over 30% of phosphorus in rivers comes from agricultural fertilizer runoff,[7] while nitrogen significantly contributes to water eutrophication and declining drinking water quality.[8]

Numerous studies have explored strategies and formulations to regulate nutrient release and overcome the limitations of

Received: April 29, 2024
Revised: January 10, 2025
Accepted: January 14, 2025
Published: January 24, 2025

ACS Publications

© 2025 The Authors. Published by American Chemical Society

https://doi.org/10.1021/acsagscitech.4c00243
ACS Agric. Sci. Technol. 2025, 5, 142−157

NPK-based fertilizers. Coating fertilizers with low-permeability materials has proven slow nutrient release and enhance efficiency. For example, slow-release nitrogen strategies use polymer coatings on urea granules to prevent rapid dissolution.[9,10] Urea-aldehyde with hydrolytic properties and blends with hydrogels have also been used to mitigate nitrogen loss.[11,12]

Phosphorus efficiency in agriculture remains notably low, typically ranging from 15 to 30%.[13,14] The increased demand for P-fertilizers, coupled with the declining availability of natural phosphorus resources, has driven a growing focus on improving their efficient use.[15] Coated phosphate fertilizers, often with polymers as coating materials, have been proposed as a solution.[16] Nevertheless, studies indicate that these coatings frequently provide a phosphorus release period of less than one month, falling short of the standards for controlled-release fertilizers.[17] To address this, advancements such as nanomaterials, interpenetrating polymer networks, and innovative low-cost polyolefin wax have been explored to enhance the performance of these fertilizers.[18,19]

Addressing the inefficient use of other essential elements remains a significant challenge, emphasizing the importance for synthesizing multielement materials. In this context, glass fertilizers (GF) have emerged as a promising solution. Glass, a nonequilibrium, noncrystalline state of matter, is defined by the frozen amorphous structure of a supercooled liquid (SCL) with the same composition.[20] This unique structure exhibits exceptional versatility, enabling the incorporation of most elements classified as micronutrients (B, Fe, Mo, Cu, Zn, Mn, etc.) and macronutrients (P, K, Ca, Mg, etc.) except nitrogen. This compositional adaptability allows GF to be tailored to meet the specific nutritional requirements of diverse plant species.

Additionally, the GF composition can be designed to achieve controlled water solubility and gradual nutrient release over time.[21] For example, Wacławska and Szumera demonstrated that the dissolution rate of phosphate glass decreases with increasing SiO_2 concentration, showing a steady decline up to 3 mol % and a more pronounced reduction beyond 4 mol %.[7,22] These distinctive properties set GF apart from conventional fertilizers, proving advantages such as minimized bioaccumulation and reduced toxicity.

Several studies have demonstrated the advantages of GF over conventional fertilizers. Researches has investigated complex GF compositions within systems such as P_2O_5–Al_2O_3–SiO_2–Na_2O–K_2O–CaO–MgO–BaO–SrO–Fe_2O_3–TiO_2,[23] P_2O_5–Na_2O–SO_3–K_2O–CaO–MnO–BaO–Fe_2O_3–CuO–ZnO–WO_3,[24] and P_2O_5–Al_2O_3–SiO_2–K_2O–CaO–MgO–MnO–SO_3–Fe_2O_3–ZnO–B_2O_3.[5,5] For instance, GF application has notably increased tomato yields in both open field and protected cultivation conditions.[5,25,26] Tamayo et al.[5] reported enhanced tomato yield using GF compared to conventional NPK fertilizers, with no adverse effects on fruit quality. Similarly, orange trees treated with a GF in the P_2O_5–Al_2O_3–SiO_2–K_2O–CaO–MgO–MnO–Fe_2O_3–ZnO–CuO–B_2O_3 system[27] achieved adequate micronutrient levels, though yield and fruit quality remained comparable to NPK treatments. Moreover, GFs have demonstrated positive effects on other crops, including corn,[28] wheat,[3] and peas.[4]

Most studies evaluate GF solubility in citric acid solutions to mimic the low-pH conditions near plant roots that facilitate nutrient absorption. In these conditions, the acidic environment promotes nutrient leaching from the glass matrix.[7,22] Similarly, studies examining soil moisture effects on glass surface reveal a corrosion mechanism consistent with *in vitro* citric acid solution testing.[29]

SiO_2-based glasses feature a three-dimensional interconnected network of [SiO_4] tetrahedral units, which directly influences the dissolution rate.[5] Depending on the SiO_2 content, a transient silica gel layer can form on the glass surface, serving as a protective barrier that slows the release of SiO_2 and other nutrients. This phenomenon is less prevalent in phosphosilicate systems.[29,30] Although silicon is not typically classified as a primary nutrient, it enhances plant resistance to pests, nematodes, and pathogens while improving resilience to drought and salinity stress. These effects contribute to better nutritional uptake, higher transpiration efficiency, and improved photosynthesis.[21,31]

Ecotoxicology evaluation is crucial for assessing new substances, providing essential insights into their potential adverse effects on ecosystems.[32] This information is vital for environmental protection and pollution prevention. While GFs offer a promising and sustainable alternative to conventional fertilizers for precision agriculture, a deeper understanding of the correlation between their composition, structure, dissolution kinetics, agronomic performance, and ecotoxicological effects remains limited.

In this study, we present a water-soluble, multicomponent glass fertilizer with a phosphosilicate network, specifically designed for controlled nutrient release. The GF's characterization was complemented by an in-depth evaluation of its agronomic and environmental performance. Experiments included dissolution rate assessments of ground material with two granulated sizes immersed in citric acid/citrate buffer solutions. Additionally, greenhouse trials with Palisade grass (*Urochloa brizantha* cv Piatã) were conducted to examine nutrients release and dry matter production. The GF's safety and environmental compatibility were evaluated through cytotoxicity and phytotoxicity tests using *Lactuca sativa* and *Allium cepa*.

2. EXPERIMENTAL PROCEDURE

2.1. Glass Fertilizer Synthesis. A 100 g glass batch was synthesized using analytical-grade raw materials in the multicomponent system P_2O_5–SiO_2–B_2O_3–CaO–K_2O–MgO–MnO_2–MoO_3–ZnO via the conventional melt-quenching method under ambient conditions. Initially, the powdered reagents were first dried at 120 ± 0.5 °C for 12 h to eliminate adsorbed moisture. The dried powders were then weighed using an analytical balance (AUY220, Shimadzu) according to the molar concentrations listed in Table S1. After homogenization in an alumina ball mill for 2 h, the mixture was melted at 1100 °C for 2 h in a ZrO_2–Al_2O_3–SiO_2 (ZAS) crucible. The molten glass was poured onto a stainless-steel plate and pressed with another plate at room temperature to ensure rapid cooling and glass formation. Approximately 3 g of the resulting GF was retained as a pristine sample. The remaining material was ground, milled, and sieved to obtain two particle size fractions 0.85 to 2.0 mm and <0.85 mm (Figure S1). The non crystalline nature of the GF was confirmed by X-ray diffraction (XRD) analysis (Figure S2).

2.2. Nutrient Release. All laboratory glassware and flasks were thoroughly cleaned with a 10% v/v HNO_3 solution for 12 h to prevent contamination. Ground and sifted GF grains ($0.85 < x < 2.0$ mm) were accurately weighed and divided into 30 portions of approximately 1.24 g each. Fifteen portions were placed in flasks containing 50 mL of distilled water, while the remaining 15 were immersed in citric acid/sodium citrate buffer solution. The flasks were sealed with Parafilm and placed on a shaking table. The buffer solution was prepared by dissolving 19.213 ± 0.001 g of $C_6H_8O_7$

https://doi.org/10.1021/acsagscitech.4c00243
ACS Agric. Sci. Technol. 2025, 5, 142−157

(Synth PA, purity of 99.5%) and 29.410 ± 0.001 g of $C_6H_5Na_3O_7 \cdot 2H_2O$ (Vetec P.A., purity of 99.0%) in a 1 L volumetric flask, followed by dilution to the mark with distilled water. The pH was adjusted to 4.7 using 6 mol·L^{-1} NaOH solution.

The 30 flasks, divided into two groups: 15 containing distilled water (labeled as A) and 15 containing buffer solution (labeled as T). These flasks were continuously shaken at room temperature (25 °C). At predetermined intervals of 2, 4, 6, 8, 10, 12, 16, 20, 24, 28, 32, 40, 48, 56, and 64 h, 30 mL of supernatant from each flask was carefully collected and refrigerated at 3 °C. The remaining undissolved GF grains in each solution were filtered, dried at 80 ± 0.5 °C for 2 h, weighed, and stored for further analysis. The pH of the solutions was measured at room temperature using a pH meter (Tecnal TEC-2). The concentration of elements released from the glass in both A and T solutions over the immersion periods (2−64 h) was quantified using inductively coupled plasma optical emission spectrometry (ICP-OES).

For nutrient quantification by ICP-OES, 200 μL aliquots of each sample were diluted in 10 mL with 2% (v/v) HNO_3 in volumetric flasks. Standard solutions were prepared by diluting 1000 mg·L^{-1} stock solutions (Fluka, Buchs St. Gallen, Switzerland). The analysis was conducted in triplicate using an Agilent 5110 SVDV (Synchronous Vertical Dual View) ICP-OES with radial vision. Instrument settings included a 5 s reading time, a 15 s stabilization time, a nebulizer flow rate of 0.7 L·min^{-1}, and a plasma flow rate of 12.0 L·min^{-1}. Emission wavelengths, concentration ranges, and correlation coefficients for the ICP-OES analysis are summarized in Table S1.

2.3. GF Characterizations. X-ray fluorescence (XRF) analysis was performed using a PANalytical spectrometer, MiniPal 4 model, with a typical resolution of 145 eV. Scanning electron microscopy (SEM) was conducted with an OXFORD ZEISS LEO 440 SEM. The SEM operated at an electron beam voltage of 15 kV, a current of 2.82 A, and with a 200 pA probe. Before SEM analysis, the samples were coated with carbon using a Coating System BAL-TEC MED 020 under 10^{-2} mbar chamber pressure, 60 mA current, and a deposition rate of 0.60 nm/s, and were stored in a desiccator. Infrared spectroscopy (FTIR) of the undissolved glass samples was carried out using powdered samples mixed with dry KBr at a weight ratio of 1:100. The FTIR spectra were recorded using a Shimadzu spectrophotometer, model IRAffinity 1, covering the range from 400 to 4000 cm^{-1} at room temperature. Raman spectra were obtained using a micro-Raman LabRAM-HR system from Horiba Jobin Yvon with a He−Ne laser at 632.8 nm, delivering a power of 17 mW at room temperature. Differential scanning calorimetry (DSC) to characterize the GF was performed with a TA Instruments DSC Q200. Measurements were conducted from 300 to 600 °C at 10 °C.min^{-1} using aluminum crucibles under a nitrogen (N_2) atmosphere.

2.4. Greenhouse *In Situ* Trials. A greenhouse experiment was conducted to evaluate the impact of GF application on the dry mass yield and nutrient extraction of Palisade grass (*Brachiaria brizantha*) at Embrapa Pecuaria Sudeste, located at coordinates 21° 57′12″ S and 47° 51′15″ W, with an elevation of 873 m above sea level, in São Carlos, São Paulo State, Brazil. The soil used in the experiment was classified as a Typical Quartzipsamment (according to Soil Taxonomy) or Ferralic Arenosol (as per FAO terminology) as described by Calderano et al.[33] The soil surface layer, ranging from 0 to 0.2 m in depth, exhibited the following mineral composition: 727 g·kg^{-1} of sand, 84 g·kg^{-1} of silt, and 189 g·kg^{-1} of clay. Chemical properties, analyzed using the methodology of Raij et al.,[34] were as follows: pH (H_2O) 4.3, organic matter content of 12 g·L^{-1}, available P (resin) at 4 mg·L^{-1}, and K, Ca, and Mg concentrations of 0.6, 8.0, and 2.0 mmol$_c$·L^{-1}, respectively. Other properties included a cation exchange capacity (CEC) of 50 mmol$_c$·kg^{-1}, a base saturation (V) of 21%, S_SO_4 at 4 mg·L^{-1}, and the micronutrient concentrations of B, Cu, Fe, Mn, and Zn at 0.16, 0.4, 8.0, 1.1, and 0.2 mg·L^{-1}, respectively. The soil was collected, dried, and sieved into particles smaller than 2 mm. Pots were then filled with 3 kg of the prepared soil for the greenhouse experiments.

Before planting, each pot was treated with dolomite lime (Total Neutralizing Power Ratio—TNPR of 91%, containing 32% CaO and 18% MgO) at a rate of 2.55 g·kg^{-1} to elevate the base saturation to 70%. The soil was then moistened to its water-holding capacity (WHC) and incubated for 30 days before sowing Palisade grass (*Urochloa brizantha* cv Piatã). Throughout the experiment, soil moisture was meticulously maintained at WHC.

The experimental treatments included the application of GF in two granulometries: 850 μm < x < 2 mm (10 mesh) and <850 μm (20 mesh). GF was applied at three levels, represented by 0.95, 1.9, and 3.8 mg per pot, corresponding to 50, 100, and 200% of the nutritional requirements, supplying 150, 300, and 600 mg·kg^{-1} of P_2O_5, respectively. Additionally, two control treatments were included: one without GF (control) and one with soluble salts supplying 100% of the required nutrients. This resulted in a total of eight treatments: Control, 50% GF (10 mesh), 100% GF (10 mesh), 200% GF (10 mesh), 50% GF (20 mesh), 100% GF (20 mesh), 200% GF (20 mesh), and Soluble Salts. The experimental design was a randomized block design with four replicates.

Nitrogen and sulfur were provided at a rate of 44 mg-N per kg of soil using NH_4SO_4, with N accounting 20% (molar) and S-SO_4 22%. This initial supplementation was applied 15 days after seed germination, and an additional 44 mg-N per kg of soil was applied alternately after each aboveground cut, using urea (45% N) and NH_4SO_4.

The first biomass cut occurred 45 days after fertilization, with subsequent cuts made every 30 days following grass regrowth. In each instance, the collected plant material was dried using forced air circulation at 65 °C for 72 h, weighted to determine dry matter production, and ground to a particle size of <1 mm using a Wiley mill equipped with a stainless-steel blade.

All solutions were prepared using analytical-grade reagents and distilled water with a resistivity of 18.2 MΩ cm, purified through a Milli-Q system (Millipore, Bedford, MA, USA). Nitric acid, obtained from a distillation apparatus (model distillacid BSB-939-IR, Berghof, Eningen, Germany), and hydrogen peroxide solution (30 wt %, Sigma-Aldrich, Saint Louis, MO, USA) were used in sample preparation. Standard solutions were prepared from 1000 mg·L^{-1} stock solutions (Qhemis, Brazil).

Dried mass samples from each treatment were digested in a microwave oven (Multiwave Go, Anton Paar) with diluted acid for nutrient quantification. For this, a 200 mg sample were taken in triplicate, and 4 mL of 14 mol·L^{-1} HNO_3, 2 mL of 30% m·m^{-1} H_2O_2, and 2 mL of deionized water were added. The mixture underwent microwave-assisted digestion with the following heating program: (i) 20 min at 150 °C, and (ii) 20 min at 200 °C, with 10 min cooling steps between each heating cycle. After cooling to room temperature, the digested samples were adjusted to a final volume of 50 mL with deionized water. The analytes were subsequently quantified by ICP-OES, as previously described. Nutrient extraction ($Nut_{extraction}$) was calculated by multiplying the dry matter mass of each cut (DM, in kg per pot) by the respective nutrient content (NC, in mg·kg^{-1}).

The evaluation of GF in different levels and granulometry was conducted calculating the agronomic efficiency (AE, %), using the equation from Chien et al.:[35] $\text{AE}\,(\%) = \frac{(Y_{\text{treatments}} - Y_{\text{control}})}{(Y_{\text{soluble salts}} - Y_{\text{control}})} \times 100$, where Y represents Palisade grass yield (g per pot) for each treatment in relation to Y soluble salts fertilization, and Y-control represents the Palisade grass yield (kg per pot) for the control treatment with no nutrient.

Soil chemical properties were determined after the fifth cut using methods outlined by Raij et al.:[34] pH ($CaCl_2$), organic carbon (wet combustion), available P (resin method), exchangeable K^+, Ca^{2+}, Mg^{2+} and H+Al, cation exchange capacity (CEC), base saturation (% V), and micronutrients Cu, Fe, Mn, and Zn (DTPA).

Statistical data analysis was performed using SAS 9.4 (SAS Institute, Inc., Cary, NC). Differences between treatments were evaluated using a randomized block analysis of variance (ANOVA) with significance set at $p < 0.05$. Tukey's test ($p < 0.05$) was used to compare treatment means.

https://doi.org/10.1021/acsagscitech.4c00243
ACS Agric. Sci. Technol. 2025, 5, 142−157

2.5. Ecotoxicological Evaluation of the Glass Fertilizer. The ecotoxicological potential of GF was assessed using two granulometries: 10 mesh and 20 mesh (ranging from 2 mm to 850 μm). Five distinct GF concentrations were evaluated: 0.317 g·kg^{-1} (Cc1), 0.633 g·kg^{-1} (Cc2), 1.267 g·kg^{-1} (Cc3), 2.534 g·kg^{-1} (Cc4), and 5.063 g·kg^{-1} (Cc5). Concentrations Cc1, Cc2, and Cc3 corresponded to 50, 100, and 200% of the phosphorus nutritional requirements employed in the greenhouse *in situ* trials. Concentrations Cc4 and Cc5 were progressively increased by a factor of 2 from the initial values. For the evaluation, GF was precisely weighted using an analytical balance and directly incorporated into the soil. The soil used in these evaluations was the same as that described in Section 2.4. After the GF was added, the soil was thoroughly homogenized to even ensure uniform fertilizer distribution.

2.5.1. Phytotoxicity Test with Lactuca sativa. The phytotoxic potential of the samples was assessed following the OPPTS 850.4200 protocol guideline.[36] *Lactuca sativa* is commonly used for phytotoxicity evaluations due to its high sensitivity to environmental stressors induced by toxic substances. This species is a standard for assessing key parameters such as germination rate, radicle length, and hypocotyl length.[37,38]

Twenty *L. sativa* seeds (Wanda variety) were evenly distributed in individual Petri dishes containing 50 g of soil and one of five tested GF concentrations, each in one of two granulometries. The soil moisture content was adjusted to 70% of its field capacity by adding 9.2 mL of water per plate. Negative control (NC) plates, containing soil at 70% of field capacity, were used exclusively. Positive control (PC) plates were treated with 0.05 M zinc sulfate heptahydrate ($ZnSO_4{\cdot}7H_2O$).

The plates were incubated at 22 ± 2 °C in the dark for 120 h. The experiment was conducted in triplicate. After this period, the number of germinated seeds (defined by a radicle size greater than 5 mm) was recorded, and the hypocotyl and radicle lengths of each germinated seed were measured. Based on these data, Relative Germination (RG), Root Relative Growth Rate (RR), and the Germination Index (GI) were calculated using the equations proposed by Tiquia[39]

$$\text{RG (\%)} = \frac{\text{Number of germinated seeds in the sample}}{\text{Number of germinated seeds in the control}} \times 100$$

$$\text{RR (\%)} = \frac{\text{Average growth of sample roots}}{\text{Average growth of control roots}} \times 100$$

$$\text{GI (\%)} = \frac{\text{RG} \times \text{RR}}{100}$$

The concentrations were categorized based on their toxicity levels as follows: nontoxic (GI > 80%), moderately toxic (GI between 30 and 80%), and highly toxic (GI < 30%), according to the classification proposed by Gonçalves et al.[40] Statistical analysis was performed using the Kruskal–Wallis test, with a significance level set at $p < 0.05$, employing the BioEstat 5.1 software.

2.5.2. Cytogenotoxicity Test with Allium cepa. In the experiments with *A. cepa*, 50 seeds of the Híbrida Diamantina variety were evenly distributed in individual Petri dishes, each containing 50 g of soil supplemented with varying concentrations of GF in two distinct granulometries. Untreated soil was used for the NC, while the PC was supplemented with methylmethanesulfonate at a concentration of 10 mg/L (MMS, Sigma-Aldrich, CAS 66-27-3). The soil moisture content in each dish was adjusted to 70% of its field capacity by adding 9.2 mL of ultrapure water for the test samples and NC, or 9.2 mL of the MMS solution for the PC.

The Petri dishes were incubated in a BOD chamber for 120 h at 22 ± 2 °C, with a 12 h photoperiod. The experiment was conducted in triplicate. After the incubation period, rootlets were collected, fixed in Carnoy's solution (ethanol/glacial acetic acid, 3:1, v/v) for 6 h, and then transferred to fresh fixative for long-term storage at 4 °C.

Preparation and analysis of meristematic cell slides followed the protocol by Grant (1982) with minor adjustments. After removing excess fixative by rinsing with distilled water, the roots were subjected to acid hydrolysis with 1 N HCl for 10 min, followed by DNA labeling using Schiff's reagent for 2 h.

After removing any surplus dye, the rootlets were placed on slides, and the meristematic region was carefully sectioned with a scalpel. The meristematic area was then covered with a 2% acetic carmine drop and a coverslip. Gentle pressure was applied to promote cell spreading. The coverslips were subsequently removed using liquid N_2, and the material was covered with synthetic resin and an additional coverslip to create permanent slides.

The slides were examined using a light microscope at magnifications ranging from 400× to 1000×. Cytotoxicity was assessed by calculating the mitotic index (MI), which is the ratio of dividing cells to the total number of cells analyzed. Additionally, various cellular alterations were considered, including chromosomal losses, breaks, adhesions and bridges, micronuclei, nuclear buds, polyploid cells, and other anomalies observed during the mitotic cell cycle. These alterations were considered as genotoxic changes.

Approximately 500 cells were counted per slide, with four slides examined per Petri dish, resulting in 12 slides per concentration (c.a. 6000 cells per treatment). Statistical analysis was conducted using the BioEstat 5.1 software, with significance determined using the Kruskal–Wallis test at a significance level of 0.05.

3. RESULTS AND DISCUSSION

The release rate and mechanisms governing nutrient liberation from GF are influenced by the glass dissolution process, which occur via two primary pathways: (i) ion exchange and (ii) hydrolysis reactions.[21,41] Figure 1 illustrates a hypothetical

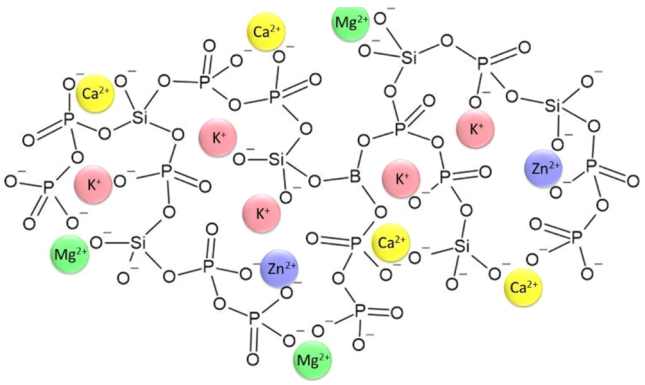

Figure 1. Schematic representation of a glass structure considering P_2O_5, SiO_2, and B_2O_3 as formers, with the addition of K^+, Ca^{2+}, Mg^{2+}, and Zn^{2+} as stabilizers of nonbridging oxygens atoms.

glass structure that approximates the composition used in this study, comprising three glass formers—P_2O_5, SiO_2, and B_2O_3—in a 14/6/1 ratio. In this structure, $[PO_4]_n$, $[SiO_4]_n$, $[BO_4]_n$, and $[BO_3]_n$ units are interconnected via shared corners, with $[BO_4]_n$ tetrahedra and $[BO_3]_n$ planar trigonal units forming depending on the boron concentration.[42] Ion-exchange reactions are influenced by the prevalence of ionic-bond components within the glass network. Ions such as K^+, Ca^{2+}, Mg^{2+}, and Zn^{2+} are preferentially released through ion exchange with H_3O^+ from the aqueous environment. Hydrolysis, on the other hand, begins with the formation of terminal hydroxyl groups (P–OH, Si–OH, and B–OH) and nonbridging oxygens, leading to glass network dissolution and the generation of water-soluble species like H_4SiO_4, H_3PO_4, and H_3BO_3.[21,43]

The molar percentages of the elements determined by XRF are summarized in Table 1, with most values closely aligning with the nominal composition. The absence of boron in the

https://doi.org/10.1021/acsagscitech.4c00243
ACS Agric. Sci. Technol. 2025, 5, 142–157

Table 1. Theoretical (Calculated) and Experimental Molar Percentages (mol %) of the Elements in the GF, Based on Their Oxide Form

oxides	calculated (mol %)	experimental XRF (mol %)	initial mass of cations in 1.24 g (mg)
P_2O_5	41.23	46.34	345.1
CaO	19.32	14.89	71.7
SiO_2	14.52	12.60	42.6
K_2O	9.70	10.49	98.6
ZnO	5.81	7.25	57.0
MgO	5.07	3.59	10.5
B_2O_3	2.90	2.90[a]	7.5
MnO_2	0.97	1.02	6.7
MoO_3	0.49	0.92	10.6

[a]Note: did not detect B_2O_3; its calculated mol % was used to normalize the concentrations.

analysis is due to the low sensibility of XRF for elements with a low atomic number ($Z \leq 10$). This limitation required normalizing the nominal molar concentrations presented in Table 1 to compensate for the absence of B_2O_3. The semiquantitative nature of XRF accounts for the differences between the theoretical and experimental contents. In this analysis, the intensity of the emitted X-rays for a specific element is influenced by the absorption effects of other elements within the sample, disrupting the linear correlation between X-ray intensity and elemental concentration.[44] Despite these limitations, all oxide elements in the GF studied were detected, with the exception of boron.

The variation in GF mass over different immersion times in water and buffer solutions is depicted in Figure 2a. The recorded values, with a standard deviation of ±0.001 g, indicate a consistent reduction in GF mass as immersion time increases. However, the dissolution behavior in water and buffer solutions exhibited significant differences in the early stages of the dissolution processes.

In the first 2 h, the GF in water experienced a sharp decrease in mass, similar to the trend observed in the buffer solution. This was followed by a period of stability until 6 h. After this point, the mass decreased steadily in a linear fashion until the experiment concluded at 64 h. In contrast, the GF in the buffer solution exhibited a continuous, nonlinear decrease in mass during the initial stages of dissolution. After approximately 12 h, the dissolution behavior in the buffer solution aligned with the linear pattern observed in water, although at a slightly higher rate.

The GF samples immersed in water (A) experienced a lower overall mass loss over 4 h than those in the buffer solution (T). The A64 and T64 samples exhibited the most significant reductions, with 39 and 54% mass loss, respectively. The constant mass-loss rates were determined using the tangents of the linear fits to the data, starting after 6 h for water and after 12 h for the buffer solution. For the A samples, the rate was 0.0073 ± 0.0002 g·h^{-1} (with an intercept at 1.218 h and R^2 = 0.99), and for the T samples, It was 0.0078 ± 0.0006 g·h^{-1} (with an intercept at 1.0457 h and R^2 = 0.95). The time required for total dissolution (t_{TD}) can be estimated using the linear fitting equations by setting the mass equal to zero, allowing for the respective calculation of dissolution times in water (t_{TD_A}) and buffer solution (t_{TD_T})

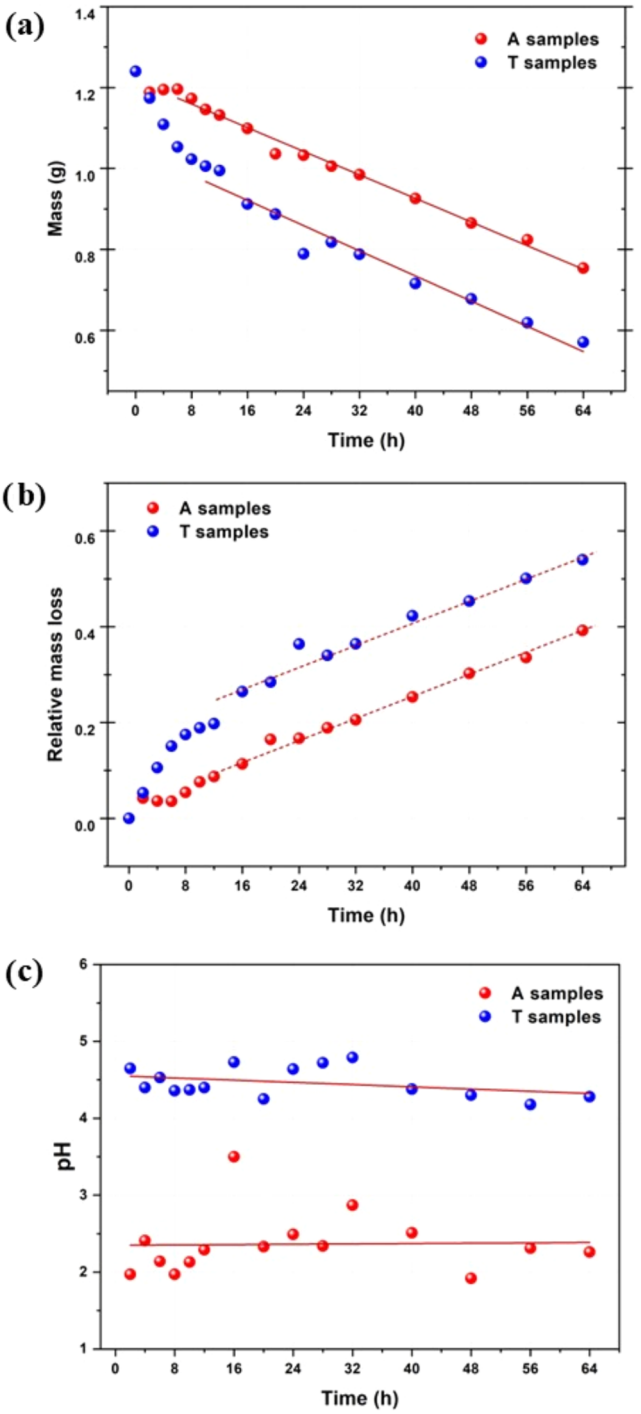

Figure 2. GF mass loss (a), relative mass loss (b), and pH behavior (c) versus immersion time in water (A) and buffer solution (T).

$$t_{TD_A} = \frac{1.218}{0.0073} = 167 \text{ h} = 7.0 \text{ days}$$

$$t_{TD_T} = \frac{1.0457}{0.0078} = 134 \text{ h} = 5.6 \text{ days}$$

In accordance with the hypothesis of complete dissolution, the samples immersed in the citric acid/sodium citrate buffer solution are expected to dissolve more rapidly, with an estimated dissolution time of 134 h (approximately 5.6 days). In contrast, the samples immersed in water are anticipated to exhibit a longer dissolution time of 167 h (about 7.0 days) to

https://doi.org/10.1021/acsagscitech.4c00243
ACS Agric. Sci. Technol. 2025, 5, 142−157

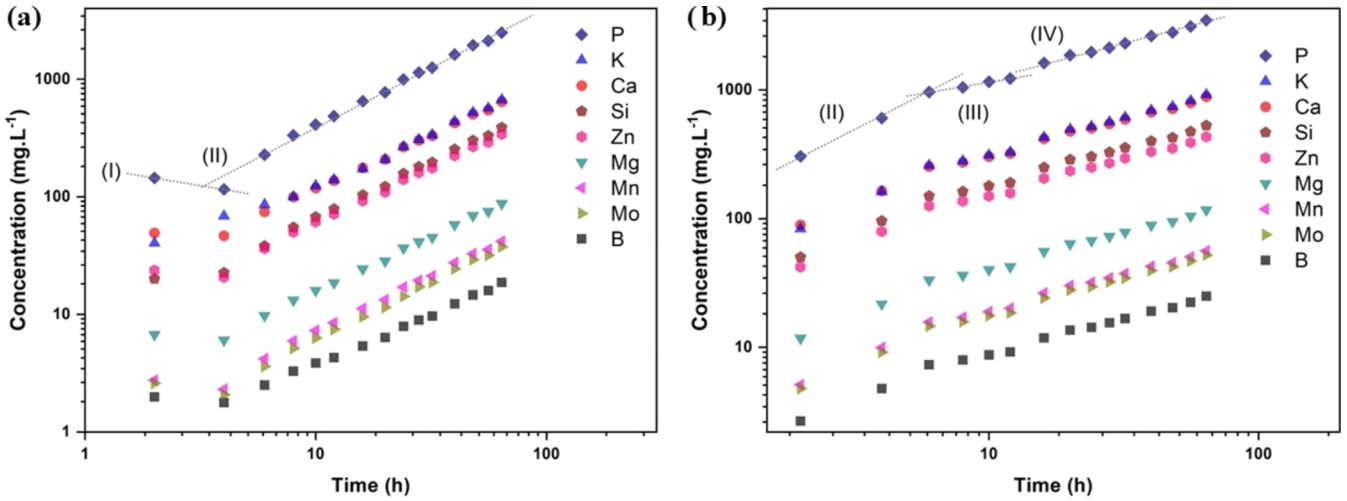

Figure 3. Logarithm plot of the concentration of the GF's elements released in (a) water (A) and (b) citric acid/sodium citrate buffer (T) solutions as a function of immersion time. The dashed lines serve as visual guides, indicating the overall trends.

reach completion. This difference in dissolution rates is depicted in Figure 2a.

Figure 2b presents the data from Figure 2a, rearranged to show the relative mass loss, calculated as the difference between the initial mass and the mass at a given immersion time, relative to the initial mass. This representation underscores the dissolution behavior previously discussed in Figure 2a, offering a clearer understanding of the mass loss dynamics. Furthermore, this depiction anticipates the trends shown in Figure 3, where a gradual increase in the concentration of individual elements released in both solutions is observed over time.

The soil's buffering capacity and slight acidity in the pH range of 4 to 7, provided the rationale for using a citric acid/sodium citrate buffer solution to simulate natural soil conditions. This solution is particularly effective, within the pH range of 3.7 to 5.7. For this study, the solution was adjusted to a pH of 4.7, corresponding to the pK_a of citric acid. During the dissolution experiment, the buffer solutions exhibited slight pH fluctuations between 4.2 and 4.8. Most buffer solutions experienced a pH drop after adding GF grains, indicating moderate acidification that persisted throughout immersion. In contrast, a larger pH fluctuation was observed when GF was dissolved in water, with a significantly lower pH ranging from 1.9 to 3.5. Figure 2c illustrates the strongly acidic nature of GF in water, with an average pH of 2.4 ± 0.2. In contrast, the buffer solution maintained a relatively constant pH, averaging 4.5 ± 0.1, regardless of the amount of GF dissolved. This stability suggests a buffering effect of the solution.

Figure 3 exhibits the concentrations of GF elements after dissolution in water and buffer solutions, as determined by ICP-OES, plotted as a function of the immersion time. The concentrations exhibit approximately linear trends over time, with stages exhibiting different slopes, as observed in the log−log scale. These stages, labeled as (I) to (IV) in Figure 4, suggest the presence of distinct dissolution mechanisms or kinetics during the experiment.

Figure 4 shows the dissolution-rate constants, defined by the slopes of the linear fits in the different dissolution stages indicated in Figure 3 for both water and buffer solutions. The highest variability is observed in stage (I) for GF immersed in

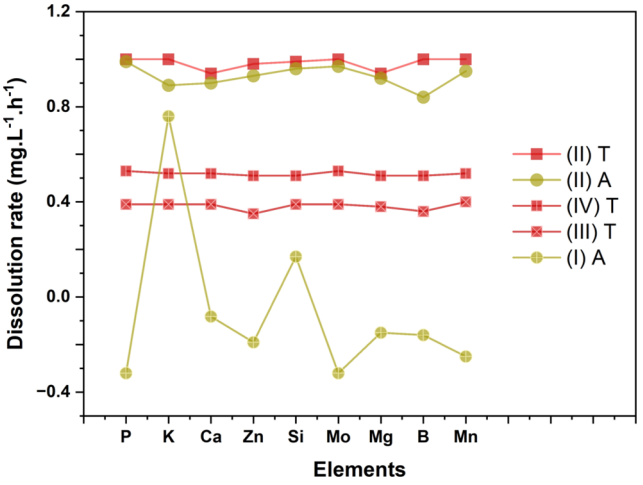

Figure 4. Dissolution constants corresponding to the slopes of the straight lines indicated in Figure 4, fitting the data points at different stages of dissolution in water (A), and citric acid/sodium citrate buffer solution (T) for each element. The initial molar concentrations of cations in the GF (see Table S2) are presented in descending order from left to right on the horizontal axis.

water (I−A), where potassium and silicon exhibit a positive dissolution rate. At the same time, the concentration of other elements decreases after the initial 2 h of mass release. Potassium, the only alkaline ion in GF composition and the second most concentrated element after phosphorus (Table S2), follows an expected trend due to its high leachability. Following stage (I), the overall glass dissolution in water progresses into stage (II), with a consistent dissolution rate for all components until the end of the experiment. In contrast, GF components immersed in the buffer solution bypass stage (I) and directly enter stage (II), exhibiting a similar slope to that observed in water. However, the release rate decreases during stage (III), followed by a partial recovery in stage (IV). The behavior of each GF component is more clearly represented in Figure 5.

Differences among the analyzed species can be partially attributed to their concentrations in the glass composition. Their concentrations of these species in solution, normalized by their initial amount in the GF, are depicted in Figure 5,

https://doi.org/10.1021/acsagscitech.4c00243
ACS Agric. Sci. Technol. 2025, 5, 142−157

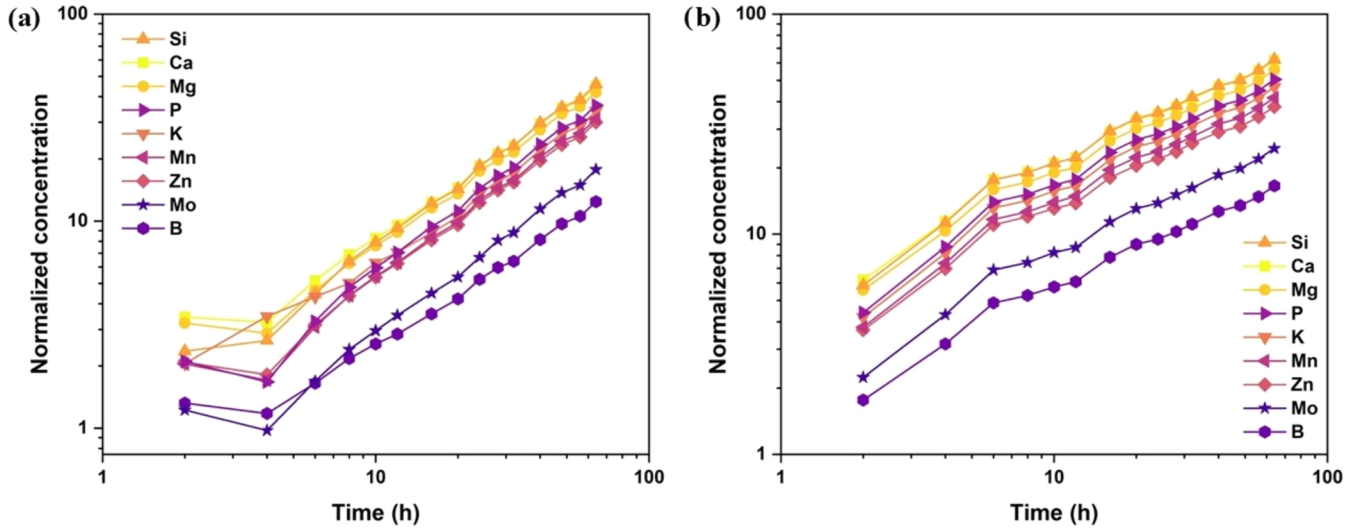

Figure 5. Normalized dissolved concentrations versus immersion time in (a) water and (b) buffer solution.

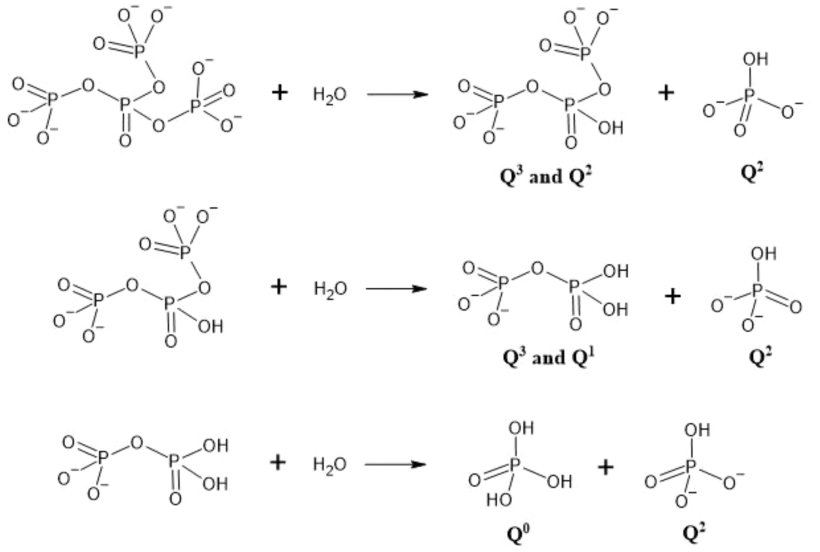

Figure 6. Schematic reactions are involved in the phosphorus dissolution process.

highlighting the ion release dynamics, which involves ion exchange and hydrolysis.[42] Overlapping data points may indicate species that are released together in the solution. Phosphorus from P_2O_5 and silicon from SiO_2 are the primary glass formers in higher concentrations within the GF. However, P is significantly more concentrated than Si (Table S2). The relatively lower concentration of P_2O_5 in the solutions may indicate that phosphorus is more readily retained within the glass network. Potassium and Ca exhibit higher concentrations than silicon in both water and buffer solutions. Calcium, Mg, and K are highly soluble species, while silicon, as a network former, is expected to display greater stability within the network due to its structural connectivity.[21]

Indeed, Figure 5a reveals an initial accelerated dissolution of K, probably due to its leaching from the GF in water. Subsequently, its dissolution appears to be associated with P, Mn, and Zn. During the early stages, Ca and Mg also exhibit signs of leaching from the GF in water, but their dissolution is more closely linked with the release of silicon, which then becomes the dominant element in the overall dissolution process. In the buffer solution (Figure 5b), the initial leaching of Ca, Mg, and K observed in water is absent. Instead, the dissolution of Ca and Si from the GF appears to be closely connected, while K's dissolution seems to be associated with P_2O_5, although this relationship is less pronounced. In the buffer solution, all GF elements seem to be released through parallel mechanisms.

As illustrated in Figures 5a,b, boron is the least soluble element, acting as a network former. Borates with $[BO_3]$ planar trigonal units tend to be highly hygroscopic. However, various intermediate oxides in the composition alter the coordination number of boron, which can range from 3 to 4. As a result, most borates are structured as $[BO_4]$ tetrahedral units within the glass network, contributing to reduced dissolution rates.[45,46]

The initial stage of glass corrosion typically involves ion-exchange reactions between GF elements and H^+ or H_3O^+. In this process, glass modifier species are released, providing essential nutrients that plants can absorb as cationic species. In our case, these initial reactions may release K^+, Ca^{2+}, Mg^{2+}, Mn^{4+}, and Zn^{2+}. Alkaline and alkaline earth metals, due to their low first ionization energies, tend to form electrolytes that

https://doi.org/10.1021/acsagscitech.4c00243
ACS Agric. Sci. Technol. 2025, 5, 142−157

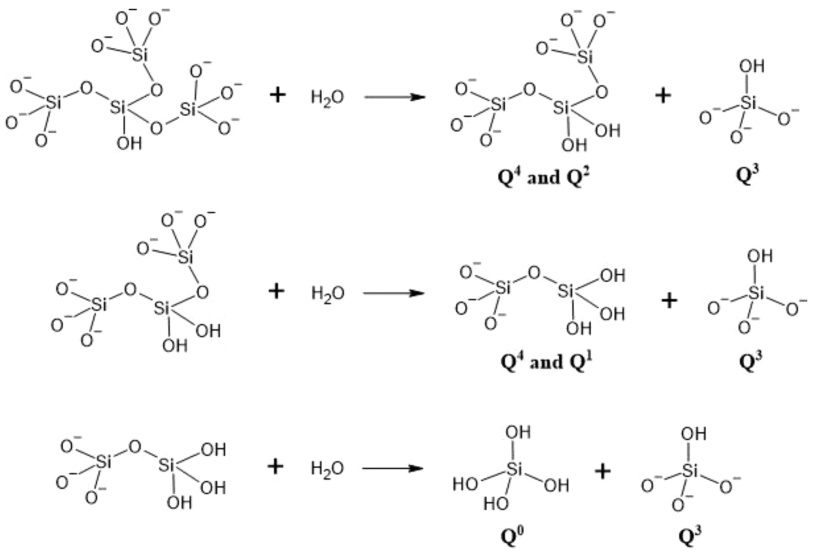

Figure 7. Dissolution and hydrolysis reactions of SiO_2.

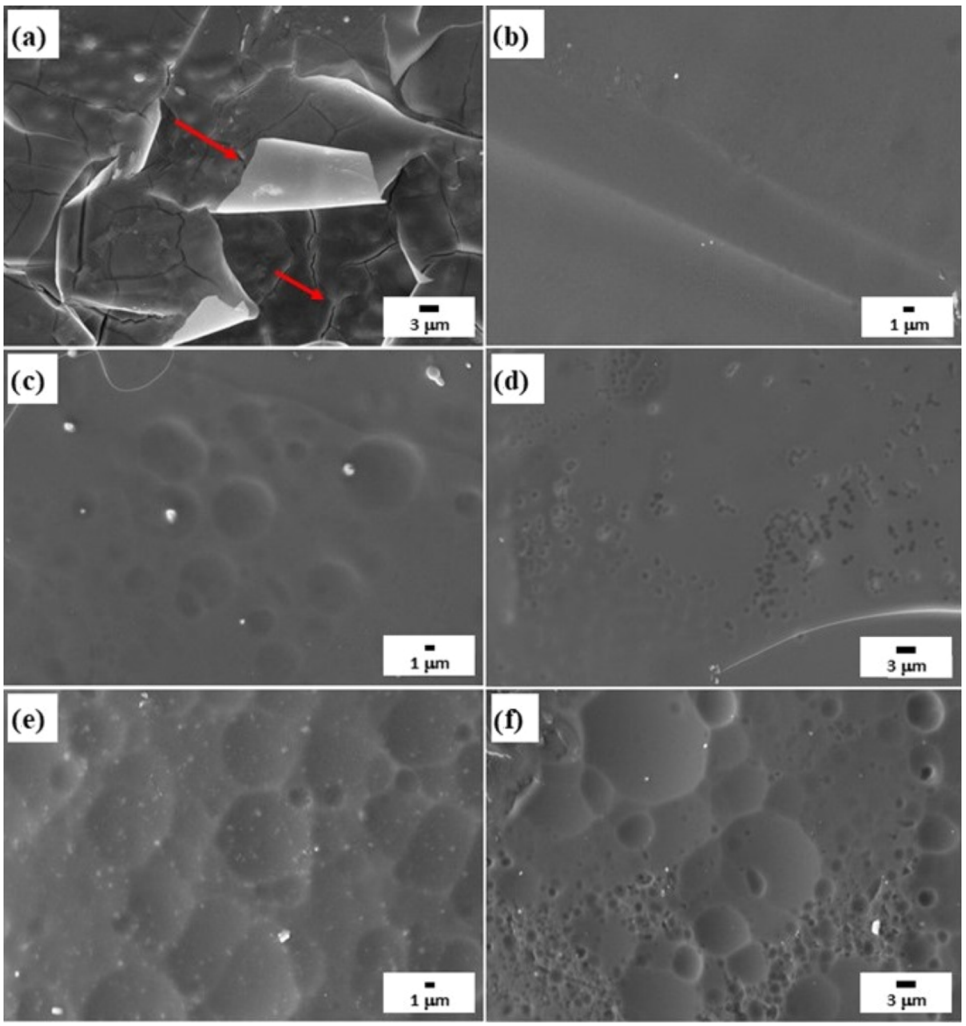

Figure 8. SEM images of samples (a) A4, (b) T4, (c) A24, (d) T24, (e) A64, and (f) T64.

solvate easily in water, enhancing their solubility when exposed to an aqueous medium. This mechanism elucidates the higher dissolution rate of GF in citric acid/sodium citrate buffer solution compared to water. The initial pH of the buffer solution was 4.7, while that of water was 6.8. The buffer solution, with more available protons, facilitated the ion-exchange mechanism and enhanced nutrient release.[21] Upon adding GF, the pH of the water solution dropped below 2.5

https://doi.org/10.1021/acsagscitech.4c00243
ACS Agric. Sci. Technol. 2025, 5, 142−157

and remained low throughout the dissolution process. This pH decrease likely offers protective effects, enabling cation leaching without disrupting the silica network. Depletion of surface cations reduces the dissolution rate, which depends on the diffusion of cations and H^+ within the particle's surface layer. Although a "pH increase" from cation leaching was not directly observed, excess OH^- could compromise the silica network. The acidification of the water solution may result from the initial breaking of bridging-oxygen within the P_2O_5−SiO_2−B_2O_3 network on the surface, consuming OH^- from the solution and enriching it in H^+. This process facilitates cation leaching, further consuming H^+, which drives a cyclic process, increasing the solution's basicity. The buffer solution initiates a similar process at a higher pH, reaching the excess OH^- stage earlier, thus accelerating the dissolution rate. The second step of the dissolution involves hydrolysis reactions, which are primarily responsible for releasing glass network formers such as P, Si, and B species. Hydrolysis reactions generate reactive hydroxyl groups on the GF particle surface, enabling the formation of soluble oxide species that dissolve into the aqueous medium. Phosphorus release from the glass forms phosphoric acid and its derivatives, including H_3PO_4, $H_2PO_4^-$, and HPO_4^{2-}. The dissolution reactions for phosphorus from the glass network are depicted in Figure 6, where negatively charged ions indicate bridging oxygen atoms that connect the amorphous structure. Metaphosphate (Q^2), pyrophosphate (Q^1), and orthophosphate (Q^0) units are formed by hydrolysis, with Q^0 units representing the H_3PO_4, $H_2PO_4^-$, and HPO_4^{2-} species released from the network.[21,47] Boron, the element with the lowest dissolution rate, is released in the form of H_3BO_3, $H_2PO_3^-$, and $H_4BO_4^-$ species under aqueous conditions.[43] It is suggested that both [BO_3] planar trigonal and [BO_4] tetrahedral units exist within the GF glass network, hindering the hydrolysis of connected groups and thus limiting the dissolution of boron within the amorphous glass network.[45,46]

As one of the primary glass formers, silica plays a crucial role in regulating the nutrient-release rates of essential cations like Ca^{2+}, K^+, Mg^{2+}, Mn^{4+}, and Zn^{2+} by stabilizing the nonbridging oxygens within the vitreous network. Figure 7 summarizes the dissolution process of the silicon oxide network, which is similar to that of phosphorus oxide but also involves the formation of Q^4 species. During hydrolysis reactions, silanol groups (Si−OH) are formed, leading to the release of silicon as silicic acid (H_4SiO_4) and its hydrolyzed species. This process mirrors the release of phosphorus species but also reflects the unique characteristics of silicon as a network former in glass dissolution.[21,31]

Molybdenum oxide is present in the GF structure at a low molar composition of 1 mol %. Previous studies on molybdenum-phosphate and tungsten-phosphate glasses have shown that the formation of [MoO_6] and [WO_6] octahedral units within phosphate chains occurs only at high concentrations of molybdenum and tungsten oxides, typically exceeding 50 and 30 mol %, respectively. At these concentrations, the glass network connectivity increases, leading to a higher glass transition temperature (T_g) due to the formation of P−O−Mo and P−O−W bridging bonds.[48,49] In this study, molybdenum oxide functions as a network modifier rather than being as integral part of the glass network. It is released as molybdic acid (H_2MoO_4) and its hydrolyzed species during dissolution.[21,50] The primary advantage of utilizing a phosphosilicate glass host as a GF rather than traditional NPK fertilizers lies in its ability to incorporate all essential micro- and macronutrient elements into a single-phase, multicomponent material. This glassy material enables a slower and more controlled nutrient release compared to conventional NPK fertilizers, with the release rate adjustable through modifications to the glass composition.[5,22,29]

To investigate the undissolved GFs and understand the mechanisms of glass dissolution, a series of characterizations were conducted. Pristine samples A4, A24, A64, T4, T24, and T64 were selected to represent short, medium, and long immersion times in water (A) and buffer solution (T). Figure 8 displays scanning electron microscope images of these sample sets, highlighting surface changes over time. Sample A4 (Figure 8a) exhibits initial signs of dissolution, including cracking and delamination (indicated by red arrows). Similar surface corrosion features, characterized by a moon-like pattern, were observed across other water-immersed samples. Sample T4 (Figure 8b), however, displayed greater resistance to cracking and delamination, with less intense corrosion, evidenced by shallow and smaller craters. As immersion time increased, samples A24 and A64 (Figure 8c,e), revealed progressively larger and deeper craters, indicative of significant surface degradation. Conversely, samples T24 and T64 displayed a broader size distribution of cavities and corrosion pit sizes, suggesting a less uniform but overall, less aggressive dissolution process in the buffer solution.[21]

Examining the surface morphology evolution over time for the A and T sample sets, as shown in Figure 8, reveals the distinct corrosion behaviors resulting from exposure to different aqueous conditions (water and buffer solution). Samples immersed in pure water exhibited more intense and uniform corrosion, characterized by moon-like patterns and larger, more prominent craters. This trend correlates with the initially sharper pH drop observed in the water solutions, reflecting the aggressive dissolution conditions.[21]

The FTIR and Raman spectra, shown in Figure S3, were recorded to evaluate the occurrence of any significant structural changes in the GF following the dissolution experiments. The spectra revealed no significant differences related to dissolution time, suggesting that these methods did not detect changes at micro- and nanometric scales on the glass surface. Both spectroscopies effectively characterized the structural features of the overall glass network. The FTIR spectra exhibited overlapping bands originating from the vibrations of [SiO_4] and [PO_4] units in the phosphate-silicate glass network. Bands around 750 and 1100 cm^{-1} correspond to the symmetric and asymmetric nonbridging oxygens stretching vibrations of P−O−P, Si−O−Si, and Si−O−P bonds in Q^1 species.[22] The band around 930 cm^{-1} may result from P−O−P symmetrical stretching vibrations in Q^2 species, while the asymmetric stretching vibrations of terminal $Si-O^-$ groups are associated with broken bonds.[29] Bands at approximately 1300 cm^{-1} relate to P═O bonds and the asymmetric stretching vibrations of P−O−P and Si−O−P in Q^2 species.[22,29] Additionally, the band around 520 cm^{-1} is assigned to deformation modes of [PO_4] tetrahedra. In addition, the bands at around 1630, 2320, and 3450 cm^{-1} are attributed to−OH groups.[51]

From the Raman spectra, the band at 330 cm^{-1} is assigned to the bending of [PO_4] units with a cation acting as a modifier.[51] Bands around 720 cm^{-1} correspond to the P−O−P symmetrical stretching vibrations in Q^1 species.[29,52] The band around 960 cm^{-1} is attributed to the [PO_4] asymmetric

https://doi.org/10.1021/acsagscitech.4c00243
ACS Agric. Sci. Technol. 2025, 5, 142−157

stretching vibrations in Q^0 species, while the at 1090 cm^{-1} represents the symmetric stretching mode of the P−O−P nonbridging bond in Q^1 species.[51,52] Bands between 1160 and 1240 cm^{-1} are related to the stretching of the nonbridging oxygen from Si−O^- bonds and to the symmetric and asymmetric stretching motions of nonbridging oxygen atoms from O−P−O bridges in Q^2 species.[51−53] Additional bands observed between 1190 and 1280 cm^{-1} are attributed to strained structural units, such as three- or four-membered rings, and the P═O symmetric stretching.[52] The band at 1280 cm^{-1} can also be related to the stretching of single nonbridging oxygen in $[SiO_4]$ tetrahedron in Q^3 species, which originate from the presence of network-modifying cations.[53]

Similarly, the DSC analysis presented in Figure S4 does not indicate significant alterations in the glass transition temperature (T_g) with varying dissolution duration. The determined T_g falls within the 450 to 500 °C range, aligns with the typical values for silicate-phosphate glasses.[54] This stability in T_g suggests that the dissolution process is restricted to the surface of the glass particles, leaving the bulk glass network unaffected.

B. brizantha (Palisade grass) stands out among forage plant species widely used in animal feed due to its high adaptability, significant biomass production, and strong regrowth capacity. However, maintaining its nutritional value requires proper management and fertilization, as the plant quickly loses its nutritional properties during early development without adequate care.[55] The dry matter yield (DMY) of Palisade grass cuts provides a valuable measure of its growth response to GF, with each of the five cuts indicating the effects of GF levels and particle granulometry. Figure 9 illustrates the statistically significant differences in DMY for the first cut (C1), influenced by both GF levels and granulometry. During the initial growth stage cycle (C1), water-soluble salts outperformed GF, resulting in significantly higher DMY due to the rapid availability of nutrients from soluble salts. However, as growth progressed to the second (C2) and third cuts (C3), GF levels exhibited a direct, statistically significant effect, while GF particle granulometry differences were not statistically significant. In later stages (C4 and C5), the main distinction was between treatment with GF and the control group. When analyzing the cumulative DMY across all five cuts, GF doses showed a significant impact, while granulometry differences remained statistically insignificant. Higher GF doses consistently led to increased DMY, regardless of particle size (Figure 9a). Overall, GF-treated groups exhibited significantly higher total DMY than the control group, with approximately 70% greater cumulative yield across all five cuts. This highlights the potential of GF to enhance forage production over an extended growth period.

The positive effects of incorporating GF on plant growth and yield, as shown in Figure 9, align with findings from previous studies. Labbilta et al.[26] conducted greenhouse experiments that demonstrated the positive effects of GF supplementation on wheat growth and production. Similarly, field studies by Rubio et al.[25] and Tamayo et al.[5] demonstrated that the highest tomato yields were achieved through the application of GF, underscoring its potential as an effective fertilizer across diverse agricultural systems.

Water-soluble nutrient sources typically exhibit faster nutrient release, especially during the initial stages of cropping cycles. However, extensive studies by Labbilta et al.,[26] Abou-Baker et al.,[28] Ait-El-Mokhtar et al.,[3] and Sayed & Ouis[4] have consistently shown that GFs can provide comparable or even

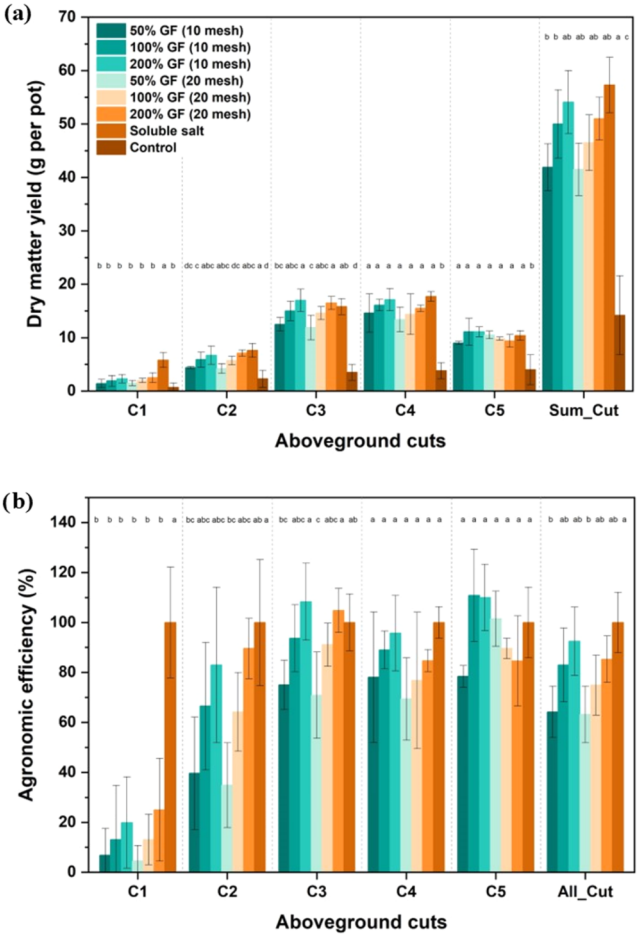

Figure 9. Palisade grass dry matter yields (a) and agronomic efficiency (b) in five cuts conducted 45 days after fertilization and after 30-day intervals following grass regrowth, and the sum of cuts encompassing the different GF levels and granulometry. Different letters indicate significant differences in Tukey's comparison test ($p < 0.05$).

superior results to soluble NPK fertilizers over multiple trials, largely due to their residual effects. Over time, the residual impact of soluble sources tends to diminish, while GF maintains their efficacy owing to their gradual and controlled nutrient solubilization. These findings highlight the effectiveness of GFs, especially in midterm experiments, where their sustained nutrient release ensures continued plant growth and productivity.

The AE index discounts the soil effect (control) and evaluates the actual output with GF relative to the standard output achieved using soluble salt. A measurement approaching 100% indicates higher source efficiency.[35] The differences observed between treatments were accentuated by the AE index. As shown in Figure 9b, the first cut exhibited a low AE (<25%) for all GF treatments, reflecting their limited initial solubilization and slow nutrient release. By the second and third cuts, AE increased, with values statistically comparable to or exceeding those of soluble salts, indicating enhanced GF solubilization and a higher nutrient release rate. No significant differences were found between the two particle sizes tested. Similarly, no differences in AE were observed among treatments during the fourth and fifth cuts. When considering all cuts collectively, significant differences in AE emerged only

https://doi.org/10.1021/acsagscitech.4c00243
ACS Agric. Sci. Technol. 2025, 5, 142−157

Table 2. Accumulated Plant Tissue P, K, Ca, Mg, Mn, Zn, and Cu for Palisade Grass Aboveground Biomass, after Five Cuts Conducted 45 Days after Fertilization and Subsequently after 30-Day Intervals Following Grass Regrowth

	(mg per pot)						(μg per pot)
treatments	P	K	Ca	Mg	Mn	Zn	Cu
control	1.7c	101.2d	66.3b	57.9b	1.57b	0.10d	0.1b
50% GF (10 mesh)	57.0b	300.6c	309.2a	224.4a	5.25a	0.82c	42.2a
100% GF (10 mesh)	91.0b	498.8ab	295.0a	225.1a	6.48a	1.56a	49.6a
200% GF (10 mesh)	135.3a	542.3a	313.9a	225.9a	6.13a	1.46ab	50.9a
50% GF (20 mesh)	52.8b	334.6cb	281.7a	221.2a	5.84a	0.98bc	42.7a
100% GF (20 mesh)	89.7b	395.1abc	318.5a	223.7a	7.66a	1.29abc	48.2a
200% GF (20 mesh)	161.3a	500.2ab	305.4a	205.3a	7.69a	1.72a	58.9a
soluble salts	76.8b	499.0ab	373.9a	276.7a	6.63a	0.96bc	61.8a

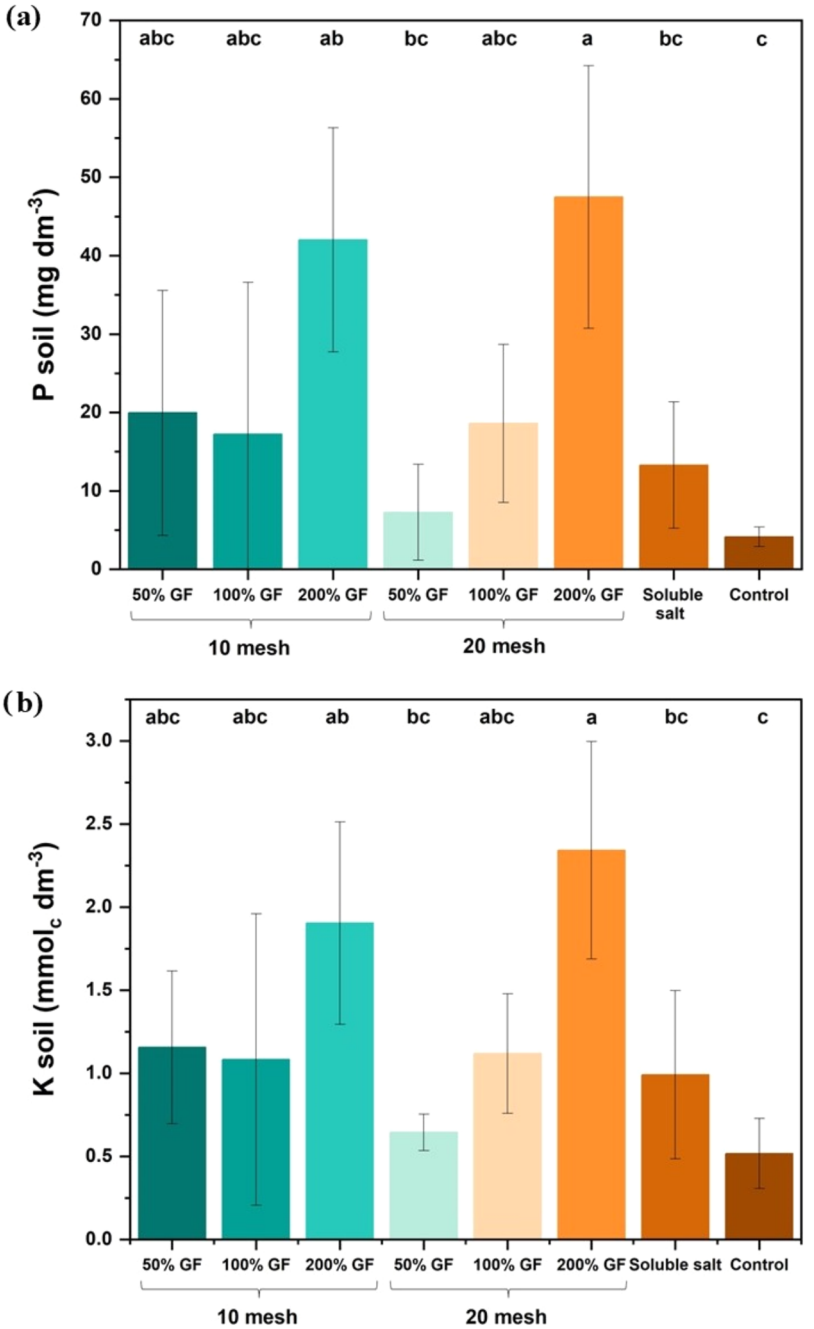
(a)
P soil (mg dm-3)
abc abc ab bc abc a bc c
50% GF 100% GF 200% GF 50% GF 100% GF 200% GF Soluble salt Control
10 mesh
20 mesh
(b)
K soil (mmolc dm-3)
abc abc ab bc abc a bc c
50% GF 100% GF 200% GF 50% GF 100% GF 200% GF Soluble salt Control
10 mesh
20 mesh

Figure 10. Residual effect of P (a) and K (b) levels in the soil at the end of the experiment.

https://doi.org/10.1021/acsagscitech.4c00243
ACS Agric. Sci. Technol. 2025, 5, 142−157

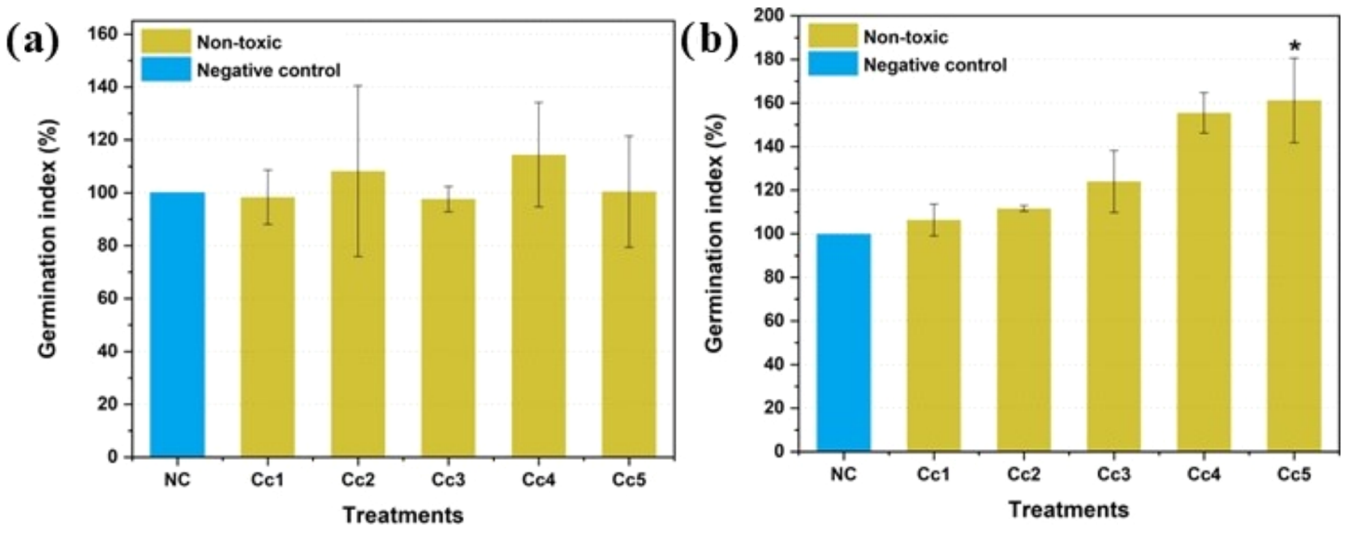

Figure 11. Comparison of germination rates in the phytotoxicity test with *L. sativa* following exposure to soil containing various concentrations of GF. (a) 10 mesh granulometry; (b) 20 mesh granulometry. NC: Negative control (soil without fertilizer addition), Cc1: 0.317 g/kg, Cc2: 0.633 g/kg, Cc3: 1.267 g/kg, Cc4: 2.534 g/kg, and Cc5: 5.063 g/kg. *Statically significant increase compared to the NC ($p < 0.05$).

at the lowest doses (50%). At 100% and 200% doses, GF performance matched that of soluble salts.

Table 2 presents the cumulative nutrient masses (P, K, Ca, Mg, Mn, Zn, and Cu) accumulated in the aboveground tissue of Palisade grass, with nutrient values expressed as the extracted quantities relative to the dry mass of each experimental pot. The results indicate that the control group consistently exhibited the lowest nutrient extraction across all five cuts. Significant statistical differences were observed in the accumulated amounts of P, K, and Zn extraction among the treatments. Higher levels of GF application resulted in significantly greater P and Zn extraction by Palisade grass, with values ranging from 135 to 161 mg per pot for P, 499 to 500 mg per pot for K, and 1.3 to 1.6 mg per pot for Zn. Conversely, no significant differences were noted in the extraction of Ca, Mg, and Cu across the treatment. These findings are consistent with those reported by Sayed & Ouis,[4] who demonstrated that GF application enhanced shoot nutrient content in peas compared to untreated plants. Similarly, Ion et al.[56] observed increased nutrient uptake in grapevines treated with glass fertilizers, especially for potassium and magnesium.

The lack of significant differences in pH, Ca, and Mg contents between treatments at the end of the experiment can be attributed to soil correction with limestone before planting and the uniform addition of fertilizers. However, statistically significant differences were observed in the P and K contents. Figure 10 illustrates the residual effect of P and K in the soil, indicating a gradual release of these nutrients. At higher GF doses (200%), the data demonstrate prolonged benefits, with significantly higher residual levels of P and K available. This gradual nutrient release ensures the availability of P (plant-available) and K (exchangeable) for subsequent crop cycles. Plants absorbed the necessary nutrients for development, while the sulfur nutrients provided by GF remained accessible for future crops. Similar long-term residual effects of GF have been reported by Rubio et al.,[25] Labbilta et al.,[26] and Ait-El-Mokhtar et al.[3]

Concerning the ecotoxicological potential of GF, the *L. sativa* test results revealed the absence of phytotoxic effects. Among higher plants, *Allium cepa* (*A. cepa*) serves as an excellent test organism for evaluating the cytotoxic and genotoxic potential of chemical substances and complex environmental samples. This is attributed to its suitable cytogenetic characteristics, ease of cultivation, and the simplicity of test implementation.[57] The germination rate of *A. cepa* seeds remained unaltered by exposure to GF, regardless of particle granulometry or concentration (Table S3). Moreover, GF did not inhibit radicle or hypocotyl growth (Figure S4), resulting in statistically similar outcomes for the evaluated treatments compared to the negative control. Additionally, treatments Cc3, Cc4, and Cc5, prepared with the 20 mesh GF, stimulated radicle and hypocotyl growth, yielding values significantly higher than those of the negative control. This positive effect is expected for fertilizers, underscoring the safety and potential of GF as a nutrient source.

The germination index (GI) classified the fertilizer as nontoxic (GI > 80%) across all tested concentrations and granulometries, including treatments Cc4 and Cc5, which exceeded the standard field application concentration by two- and 4-fold, respectively (Figure 11). Therefore, these phytotoxicity results with GF in soil underscore the high potential for agricultural applications. As highlighted by Montesano et al.,[58] the absence of phytotoxicity is a critical prerequisite for approving new products for agricultural use.

According to the results obtained in this study and information found in the scientific literature, new-generation fertilizers offer a noteworthy absence of phytotoxicity, and the numerous advantages. For instance, Wyciszkiewicz et al.[59] reported no phytotoxic effects in germination tests with *Lepidium sativum* (cress) and in the hydroponic cultivation of wheat using a phosphate-based biofertilizer obtained from the solubilization of bones by *Bacillus megaterium*. Similarly, Pantano et al.[60] demonstrated that sawdust-based fertilizers with adsorbed phosphorus are environmentally safe, showing no impact on the germination rate or the development of *L. sativa* hypocotyls and radicles. In another study, slow-release fertilizers made from hydrogels containing urea exhibited no adverse effects on the growth of garlic bean, and okra seedlings,

https://doi.org/10.1021/acsagscitech.4c00243
ACS Agric. Sci. Technol. 2025, 5, 142−157

Table 3. Percentages of Mitotic Index (MI) and the Rate of Genotoxic Alterations (RG) Acquired in the *A. cepa* Assay Following Exposure to Varying Concentrations of GF

granulometry (mesh)	effect (%)	NC	PC	Cc1	Cc2	Cc3	Cc4	Cc5
10	MI	14 ± 2	10 ± 1	11 ± 2	12 ± 2	11 ± 2	11.1 ± 0.5	12.0 ± 0.9
	RG	0 ± 0	18 ± 5[a]	0.1 ± 0.3	0 ± 0	0.2 ± 0.4	0.2 ± 0.4	0.1 ± 0.3
20	MI	10 ± 4	10 ± 3	11 ± 4	8 ± 2	11 ± 2	8 ± 4	6 ± 3
	RG	0.3 ± 0.3	6 ± 2[a]	0.5 ± 0.5	0.8 ± 0.6	0.5 ± 0.4	0.6 ± 0.5	0.5 ± 0.4

[a]Statically significant increase compared to the NC ($p < 0.05$).

further confirming the absence of phytotoxicity.[61] Additionally, fertilizers containing NPK encapsulated in polymers synthesized from poly(vinyl alcohol) (PVA) and polylactic acid (PLA) demonstrated no toxic effects on lettuce varieties grown in soil.[62] These findings underscore the reliability and environmental safety of these advanced fertilizers for cultivated plants. However, it is important to emphasize that it is essential to tailor fertilizer dosages to the specific needs of crops, as excessive nutrient supply can lead to plant toxicity.

The *A. cepa* bioassay results indicated that the fertilizer did not induce significant changes in the Mitotic Index or genotoxicity across all tested particle sizes and concentrations (Table 3). The Mitotic Index, which assesses the number of cell divisions induced by the fertilizer compared to the negative control, serves as a key parameter for evaluating cytotoxicity. A substantial increase or decrease in cell division frequency suggests potential cytotoxic properties in the tested substance.[63] Genotoxicity, which evaluates chromosomal alterations within cells, is determined by deviations in the expected frequencies of these alterations. Such deviations can result from abnormal chromosome segregation induced by factors like breaks, inhibition of DNA synthesis, or errors in replication—mechanism typically associated with anagenic or clastogenic agents.[64]

Additional studies have assessed the cytotoxic and genotoxic potential of modern fertilizers. Pantano et al.[60] reported no cytotoxic or genotoxic effects in *A. cepa* meristematic cells exposed to sawdust with phosphorus adsorption, suggesting its high potential as an agricultural fertilizer. However, it is worth noting that this sawdust contained only one nutrient type (phosphorus) at relatively low concentrations (41 $\mu g \cdot g^{-1}$). Similarly, a study examining the effects of a nanostructured polymer-based fertilizer synthesized using γ radiation on *Vicia faba* revealed no adverse effects on cell division. Genotoxicity was observed at the highest tested concentrations.[65]

Cytogenetic changes induced by fertilizers are often associated with excessive application rates and the presence of potentially toxic elements in their composition.[66] Studies on commercial nitrogen fertilizers have demonstrated that indiscriminate use can lead to chromosomal alterations in plant systems, posing genotoxic and cytotoxic risks. Evaluated nitrate levels, for instance, inhibit G1/S cell cycle progression by suppressing mitosis-regulating genes, consequently hindering cell division, reducing the mitotic index, and causing cellular damage.[67] Furthermore, research on commercial fertilizers has revealed a decrease in the mitotic index compared to control groups, accompanied by chromosomal aberrations.[68] Notably, substances known to induce genotoxicity in *A. cepa* meristematic cells have also been shown to produce similar effects in human lymphocytes, raising concerns about their broader biological impacts.[69]

In conclusion, this study investigated the dissolution mechanism and agricultural potential of a new formulation with multiple nutrients and a smart-release oxide glass design for use as a fertilizer in precision agriculture. Initial *in vitro* tests made it possible to observe the release process of the analytes in a buffered medium. The release was monitored by ICP-OES, and the characteristics of the GF were analyzed after the release study using spectroscopic techniques, FTIR, Raman, and DSC analysis. Surface morphology analysis via SEM revealed significant changes in the glass structure within the first few hours of dissolution, with a pronounced moon-like pattern developing after 64 h. These observations, coupled with spectroscopic results, indicated that dissolution was confined to the surface of the glass particles, with no notable changes in the bulk glass network.

Greenhouse experiments with *B. brizantha* (Palisade grass) demonstrated a positive and dose-dependent response to GF application. The agronomic efficiency was approximately 70% greater for GF-treated plants than the control group, with soluble salts. Increased extraction of phosphorus, potassium, and zinc was observed across the multiple cuts, highlighting the prolonged and controlled nutrient availability of GF.

No phytotoxicity was observed on seed germination or plant growth in *L. sativa* or in *A. cepa* bioassays. These results emphasize that GF, even at concentrations exceeding typical field application rates, does not pose a toxic risk to plants or cells, further supporting its suitability for agriculture use.

In conclusion, this study underscores the promising potential of GF as a sustainable and environmentally safe alternative. The dissolution mechanism ensures a controlled and gradual nutrient release supporting plant growth. The absence of adverse ecological effects and the positive impact on crop yield further highlight GF's suitability for precision agriculture, offering an efficient and long-lasting alternative to conventional fertilizers, and contributing to minimizing the environmental footprint. While this research supports the use of GF to enhance soil fertility and crop productivity, it does not claim to resolve the broader issue of overfertilization and the depletion of natural resources. We aim not to reduce the total amount applied to the soil but to extend its longevity, thereby significantly reducing the need for frequent, costly reapplications and minimizing the risk of overdissolution.

■ ASSOCIATED CONTENT

Supporting Information

The Supporting Information is available free of charge at https://pubs.acs.org/doi/10.1021/acsagscitech.4c00243.

GF grains sized between 0.85 mm and 2 mm (Figure S1); XRD pattern of the GF under study showing its noncrystalline nature (Figure S2); FTIR (a) and Raman (b) spectra of pristine (P) and A4, A24, A64, T4, T24, and T64 samples (Figure S3); Curves obtained by DSC for the pristine samples A4, A24, A64, T4, T24 and T64 (Figure S4); Length of the radicle and hypocotyl of *L. sativa* when exposed to different concentrations of GF in

https://doi.org/10.1021/acsagscitech.4c00243
ACS Agric. Sci. Technol. 2025, 5, 142−157

soil. A. 10-mesh granulometry; B. 20-mesh granulometry. NC: Negative control (soil without fertilizer addition), Cc1: 0.317 g·kg^{-1}, Cc2: 0.633 g·kg^{-1}, Cc3: 1.267 g·kg^{-1}, Cc4: 2.534 g·kg^{-1}, and Cc5: 5.063 g·kg^{-1}. *Statically significant increase compared to the NC ($p < 0.05$) (Figure S5); Concentration in the linear range of each GF element obtained by ICP OES analysis (Table S1); Raw materials, suppliers, purities, and the molar concentrations (Table S2); Seed germination rate (%) in *Lactuca sativa* following exposure to glass fertilizer (Table S3) (PDF)

AUTHOR INFORMATION

Corresponding Authors

Eduardo B. Ferreira − *São Carlos School of Engineering, University of São Paulo (EESC/USP), São Carlos 13560-970 SP, Brazil*; Email: ebferreira@sc.usp.br

Danilo Manzani − *São Carlos Institute of Chemistry, University of São Paulo (IQSC/USP), São Carlos 13560-970 SP, Brazil*; orcid.org/0000-0001-7280-5404; Email: dmanzani@usp.br

Authors

José Hermeson da Silva Soares − *São Carlos Institute of Chemistry, University of São Paulo (IQSC/USP), São Carlos 13560-970 SP, Brazil*; orcid.org/0000-0003-0787-6497

Thomaz William Boaventura − *Universidade Estadual Paulista (UNESP), Institute of Biosciences, Rio Claro 01009-906 SP, Brazil*

Ana Caroline A. de Moura − *São Carlos Institute of Chemistry, University of São Paulo (IQSC/USP), São Carlos 13560-970 SP, Brazil*

Letícia Cristina da Silva − *Center for Agricultural Sciences, Federal University of São Carlos (UFSCar), Araras 13600-970 SP, Brazil*

Amauri Garcia Filho − *Embrapa Pecuária Sudeste (EMBRAPA), São Carlos 13560-970 SP, Brazil; Chemistry Department, Federal University of São Carlos (UFSCar), São Carlos 13560-970 SP, Brazil*

Raiza L. Landgraf − *Embrapa Pecuária Sudeste (EMBRAPA), São Carlos 13560-970 SP, Brazil; Chemistry Department, Federal University of São Carlos (UFSCar), São Carlos 13560-970 SP, Brazil*

Dânia Elisa Christofoletti Mazzeo − *Universidade Estadual Paulista (UNESP), Institute of Biosciences, Rio Claro 01009-906 SP, Brazil; Center for Agricultural Sciences, Federal University of São Carlos (UFSCar), Araras 13600-970 SP, Brazil*; orcid.org/0000-0002-1696-9065

Alberto C. de Campos Bernardi − *Embrapa Pecuária Sudeste (EMBRAPA), São Carlos 13560-970 SP, Brazil*

Ana Rita A. Nogueira − *Embrapa Pecuária Sudeste (EMBRAPA), São Carlos 13560-970 SP, Brazil*; orcid.org/0000-0003-3648-2956

Complete contact information is available at: https://pubs.acs.org/10.1021/acsagscitech.4c00243

Funding

This work was supported by the São Paulo Research Foundation—FAPESP (2018/16126-7, 2023/00245-5), the Center for Research, Technology, and Education in Vitreous Materials—CeRTEV (2013/07793-6), the Conselho Nacional de Desenvolvimento Científico e Tecnológico, (CNPq project #304366/2022-6, GM/GD2020 n.157496/2021-0), the Coordination for the Improvement of Higher Education Personnel—CAPES (Finance Code 001), and Funding Authority for Studies and Projects (FINEP/CT- AGRO/FNDCT, Cooperation Agreement N. 01.22.0080.00, ref 1219/21).

Funding

The Article Processing Charge for the publication of this research was funded by the Coordination for the Improvement of Higher Education Personnel - CAPES (ROR identifier: 00x0ma614).

Notes

The authors declare no competing financial interest.

ACKNOWLEDGMENTS

We sincerely acknowledge the University of São Paulo (USP), Federal University of São Carlos (UFSCar), and the Brazilian Agricultural Research Corporation (Embrapa) for providing facilities for characterization studies, green-house experiments, and bio accessibility tests of the glass fertilizer studied in this work. We also thank the financial support from FAPESP, CNPq, and FINEP, as well as the scholarships provided by CAPES and CNPq.

REFERENCES

(1) Instituto Brasileiro de Geografia e Estatística (IBGE). Censo Agropecuário 2017. https://censoagro2017.ibge.gov.br/. Access in November 3th, 2024.

(2) Landau, E. C.; Silva, G. A.; Moura, L.; Hirsch, A.; Guimarães, D. P. Evolução da Área Ocupada por Pastagens. In *Dinâmica da produção agropecuária e da paisagem natural no Brasil nas últimas décadas: sistemas agricolas, paisagem natural e análise integrada do espaço rural*,1, 1.; Landau, E. C.; Silva, G. A.; Moura, L.; Hirsch, A.; Guimarães, D. P., Eds.; Embrapa Milho e Sorgo: Brasília, Brasil, 2020; *1*, 1556−1578.

(3) Ait-El-Mokhtar, M.; Labbilta, T.; Anli, M.; Boutasknit, A.; Abouliatim, Y.; Khouloud, M.; Mesnaoui, M.; Meddich, A. Phosphate glass-based controlled-release fertilizers improve wheat growth, yield and grain nutritional quality under field conditions. *Gesunde Pflanz.* **2022**, *74*, 715−727.

(4) Sayed, E. G.; Ouis, M. A. Improvement of pea plants growth, yield, and seed quality using glass fertilizers and biofertilizers. *Environ. Technol. Innovation* **2022**, *26*, No. 102356.

(5) Tamayo, A.; de la Torre, R.; Ruiz, O.; Lozano, P.; Mazo, M. A.; Rubio, J. Application of a glass fertilizer in sustainable tomato plant crops. *J. Sci. Food Agric.* **2018**, *98*, 4625−4633.

(6) Bokhtiar, S.; Sakurai, K. Effects of organic manure and chemical fertilizer on soil fertility and productivity of plant and ratoon crops of sugarcane. *Arch. Agron. Soil Sci.* **2005**, *51*, 325−334.

(7) Waclawska, I.; Szumera, M. Reactivity of silicate−phosphate glasses in soil environment. *J. Alloys Compd.* **2009**, *468*, 246−253.

(8) Wolfe, A. H.; Patz, J. A. Reactive nitrogen and human health: acute and long-term implications. *AMBIO: J. Human Environ.* **2002**, *31*, 120−125.

(9) Guan, Y.; Song, C.; Gan, Y. T.; Li, F. M. Increased maize yield using slow-release attapulgite-coated fertilizers. *Agron. Sustainable Dev.* **2014**, *34*, 657−665.

(10) Lyu, X.; Yang, Y.; Li, Y.; Fan, X.; Wan, Y.; Geng, Y.; Zhang, M. Polymer-coated tablet urea improved rice yield and nitrogen use efficiency. *Agron. J.* **2015**, *107*, 1837−1844.

(11) Yamamoto, C. F.; Pereira, E. I.; Mattoso, L. H. C.; Matsunaka, T.; Ribeiro, C. Slow release fertilizers based on urea/urea formaldehyde polymer nanocomposites. *Chem. Eng. J.* **2016**, *287*, 390−397.

(12) Salthammer, T.; Gunschera, J. Release of formaldehyde and other organic compounds from nitrogen fertilizers. *Chemosphere* **2021**, *263*, No. 127913.

(13) Dhillon, J.; Torres, G.; Driver, E.; Figueiredo, B.; Raun, W. R. World phosphorus use efficiency in cereal crops. *Agron. J.* **2017**, *109*, 1670−1677.
(14) Urso, J. H.; Gilbertson, L. M. Atom Conversion Efficiency: A New Sustainability Metric Applied to Nitrogen and Phosphorus Use in Agriculture. *ACS Sustainable Chem. Eng.* **2018**, *6*, 4453−4463.
(15) Davidson, D.; Gu, F. X. Materials for sustained and controlled release of nutrients and molecules to support plant growth. *J. Agric. Food Chem.* **2012**, *60*, 870−876.
(16) da Cruz, D. F.; Bortoletto-Santos, R.; Guimarães, G. G. F.; Polito, W. L.; Ribeiro, C. Role of polymeric coating on the phosphate availability as a fertilizer: insight from phosphate release by castor polyurethane coatings. *J. Agric. Food Chem.* **2017**, *65*, 5890−5895.
(17) ISO 18644−2016, Fertilizers and Soil Conditioners—Controlled-Release Fertilizer—General Requirements. https://standards.iteh.ai/catalog/standards/sist/146016f3-c2b1-470b-b59f-d2a6cc3003b7/iso-18644-2016. Access in 2th October, 2024.
(18) Ma, X.; Chen, J.; Yang, Y.; Su, X.; Zhang, S.; Gao, B.; Li, Y. C. Siloxane and polyether dual modification improves hydrophobicity and interpenetrating polymer network of bio-polymer for coated fertilizers with enhanced slow release characteristics. *Chem. Eng. J.* **2018**, *350*, 1125−1134.
(19) Lu, H.; Tian, H.; Liu, Z.; Zhang, M.; Zhao, C.; Guo, Y.; Guan, R.; Chen, Q.; Yu, X.; Wang, H.; Zheng, L. Polyolefin Wax Modification Improved Characteristics of Nutrient Release from Biopolymer-Coated Phosphorus Fertilizers. *ACS Omega* **2019**, *4*, 20402−20409.
(20) Zanotto, E. D.; Mauro, J. C. The glassy state of matter: Its definition and ultimate fate. *J. Non-Cryst. Solids* **2017**, *471*, 490−495.
(21) Hazra, G.; Das, T. A Review on Controlled Release Advanced Glassy Fertilizer. *Glob. J. Sci. Front. Res. B Chem.* **2014**, *14*, 33−44.
(22) Szumera, M. The structural role of manganese ions in soil active silicate-phosphate glasses. *Spectrochim. Acta, Part A* **2014**, *129*, 601−608.
(23) Andreola, F.; Borghi, A.; Pedrazzi, S.; Allesina, G.; Tartarini, P.; Lancellotti, I.; Barbieri, L. Spent Coffee Grounds in the Production of Lightweight Clay Ceramic Aggregates in View of Urban and Agricultural Sustainable Development. *Materials* **2019**, *12*, 3581.
(24) Kiwsakunkran, N.; Chanthima, N.; Kaewkhao, J.; Sangwaranateec, N. Composition and structural studies of glass fertilizer. *J. Phys.: Conf. Ser.* **2018**, *1120*, No. 012016.
(25) Rubio, J.; Rodríguez, R.; Ciruelos, A.; Ruiz, O.; Lozano, P. A.; De La Torre, R. New glass fertilizer for tomato crops to reduce environmental impact. *Acta Hortic.* **2017**, *1159*, 65−72.
(26) Labbilta, T.; Ait-El-Mokhtar, M.; Abouliatim, Y.; Khouloud, M.; Meddich, A.; Mesnaoui, M. Elaboration and Characterization of Vitreous Fertilizers and Study of Their Impact on the Growth, Photosynthesis and Yield of Wheat (Triticum durum L.). *Materials* **2021**, *14*, 1295.
(27) Torrisi, B.; Trinchera, A.; Rea, E.; Allegra, M.; Roccuzzo, G.; Intrigliolo, F. Effects of organo-mineral glass-matrix based fertilizers on citrus Fe chlorosis. *Eur. J. Agron.* **2013**, *44*, 32−37.
(28) Abou-Baker, N. H.; Ouis, M.; Abd-Eladl, M. Appraisal of agriglass in promoting maize production under abiotic stress conditions. *Silicon* **2018**, *10*, 1841−1849.
(29) Waclawska, I.; Szumera, M. Reactivity of silicate−phosphate glasses in soil environment. *J. Alloys Compd.* **2009**, *468*, 246−253.
(30) Abdelouas, A.; Neeway, J.; Grambow, B. Chemical Durability of Glasses. In *Springer Handbook of Glass. Springer Handbooks*. Musgraves, J. D.; Hu, J.; Calvez, L., Eds.; Springer, Cham, New York. 2019, *1*, 407−438.
(31) Menegale, M. L. C.; Castro, G. S. A.; Mancuso, M. A. C. Silicon: Interaction with the soil-plant system (in Portuguese). *J. Agron. Sci.* **2015**, *4*, 435−454.
(32) Brooks, B. W. Greening Chemistry and Ecotoxicology Towards Sustainable Environmental Quality. *Green Chem.* **2019**, *21*, 2575−2582.
(33) Calderano Filho, B.; Santos, H. G.; Fonseca, O. O. M.; Santos, R. D.; Primavesi, O.; Primavesi, A. C. Os solos da Fazenda Canchim, Centro de Pesquisa de Pecuária do Sudeste, São Carlos, SP: Levantamento semidetalhado, propriedades e potenciais. https://www.infoteca.cnptia.embrapa.br/handle/doc/44746. Access in October 2th, 2024.
(34) Raij, B. V.; Andrade, J. C.; Cantarella, H.; Quaggio, J. A. Os métodos de análise química do Sistema IAC de Análise de Solo no contexto nacional. In *Análise química para avaliação da fertilidade de solos tropicais*. 1, Raij, B. V.; Andrade, J. C.; Cantarella, H.; Quaggio, J., Eds.; IAC: Campinas, Brasil, 2001; *1*. 285.
(35) Chien, S. H.; Sale, P. W. G.; Friesen, D. K. A discussion of the methods for comparing the relative effectiveness of phosphate fertilizers varying in solubility. *Fert. Res.* **1990**, *24*, 149−157.
(36) Environmental Protection Agency (USEPA). Ecological effects test guidelines (OPPTS 850.4200): seed germination/root elongation toxicity test public draft. https://nepis.epa.gov 〉 ZyPURL. Access in 2th October, 2024.
(37) Priac, A.; Badot, P. M.; Crini, G. Treated wastewater phytotoxicity assessment using *Lactuca sativa*: focus on germination and root elongation test parameters. *C. R. Biol.* **2017**, *340*, 188−194.
(38) Mazzeo, D. E. C.; Misovic, A.; Oliveira, F. A.; Levy, C. E.; Oehlmann, J.; Marchi, M. R. R. Effects of biostimulation by sugarcane bagasse and coffee grounds on sewage sludges, focusing agricultural use: Microbial characterization, respirometric assessment and toxicity reduction. *Waste Manage.* **2020**, *118*, 110−121.
(39) Tiquia, S. M. Reduction of compost phytotoxicity during the process of decomposition. *Chemosphere* **2010**, *79*, 506−512.
(40) de Moraes Cunha Gonçalves, M.; Lopes, A. C. A.; Gomes, R. L. F.; Melo, W. J.; Araujo, A. S. F.; Pinheiro, J. B.; Marin-Morales, M. A. Phytotoxicity and cytogenotoxicity of composted tannery sludge. *Environ. Sci. Pollut. Res.* **2020**, *27*, 34495−34502 Hazra.
(41) Gin, S.; Du, J.; Ryan, J.; Vienna, J.; Schaut, R.; Smith, N.; Brauer, D.; Verney-Carron, A. Short Course on Glass Corrosion. https://ceramics.org/ceramic-tech-today/glass-short-courses-add-value-to-icg-2019/. Access in November 2th, 2024.
(42) Bunker, B. C.; Arnold, G. W.; Wilder, J. A. Phosphate glass dissolution in aqueous solutions. *J. Non-Cryst. Solids* **1984**, *64*, 291−3161.
(43) Goetschius, K. L.; Beuerlein, M. A.; Bischoff, C. M.; Brow, R. K. Dissolution behavior of ternary alkali-alkaline earth-borate glasses in water. *J. Non-Cryst. Solids* **2018**, *487*, 12−18.
(44) Nagata, N.; Bueno, M. I. M. S.; Peralta-Zamora, P. G. Mathematical methods for correction of spectral interferences and interelement effects in quantitative analysis by X-ray fluorescence (in Portuguese). *Quim. Nova* **2001**, *24*, 531−539.
(45) Zhang, A. C.; Vedishcheva, N. M.; Shakhmatkin, A. B. Vitreous Borate Networks Containing Superstructural Units: A Challenge To The Random Network Theory? *J. Non-Cryst. Solids* **1995**, *192−193*, 92−97.
(46) Zhang, Z.; Hirao, K.; Soga, N. Water corrosion behavior of densified glass. II. Borate glasses. *J. Non-Cryst. Solids* **1991**, *135*, 62−66.
(47) Hudgens, J. J.; Martin, S. W. Glass Transition and Infrared Spectra of LowAlkali, Anhydrous Lithium Phosphate Glasses. *J. Am. Ceram. Soc.* **1993**, *76*, 1691−1696.
(48) Manzani, D.; Araújo, C. B.; Boudebs, G.; Messaddeq, Y.; Ribeiro, S. J. L. The Role of Bi_2O_3 on the Thermal, Structural, and Optical Properties of Tungsten-Phosphate Glasses. *J. Phys. Chem. B* **2013**, *117*, 408−414.
(49) Manzani, D.; Besse, V.; Napoli, M.; Boudebs, G.; Ribeiro, S. J.; de Araújo, C. B. Third-order nonlinearities and other properties of molybdenum lead-pyrophosphate glass. *Opt. Mater.* **2015**, *42*, 298−302.
(50) Dieterle, M.; Weinberg, G.; Mestl, G. Raman spectroscopy of molybdenum oxides. *Phys. Chem. Chem. Phys.* **2002**, *4*, 812−821.
(51) Lai, Y. M.; Liang, X. F.; Yang, S. Y.; Wang, J. X.; Cao, L. H.; Dai, B. Raman and FTIR spectra of iron phosphate glasses containing cerium. *J. Mol. Struct.* **2011**, *992*, 84−88.

(52) Cozar, O.; Magdas, D. A.; Nasdala, L.; Ardelean, I.; Damian, G. Raman spectroscopic study of some lead phosphate glasses with tungsten ions. *J. Non-Cryst. Solids* **2006**, *352*, 3121−3125.
(53) Szumera, M. Structural investigations of silicate−phosphate glasses containing MoO_3 by FTIR, Raman and ^{31}P MAS NMR spectroscopies. *Spectrochim. Acta, Part A* **2014**, *130*, 1−6.
(54) Nayab Rasool, S.; Moorthy, L. R.; Jayasankar, C. K. Spectroscopic Investigation of Sm^{3+} doped phosphate based glasses for reddish-orange emission. *Opt. Commun.* **2013**, *311*, 156−162.
(55) Bellé, J. R.; Marchi, S. R.; Martins, D.; Sousa, A. C.; Pinheiro, G. H. R. Nutritional Value of Marandú Palisade Grass According to Increasing Coexistence Periods with Weeds. *Planta Daninha.* **2018**, *36* (36), 1−11.
(56) Ion, M.; Serdinescu, A.; Pîrcalabu, L.; Sava, M. Use of vitreous fertilizers with slow release of nutrients in viticulture. *Curr. Trends Nat. Sci.* **2012**, *1*, 101−106.
(57) Leme, D. M.; Marin-Morales, M. A. *Allium cepa* test in environmental monitoring: a review on its application. *Mutat. Res., Rev. Mutat. Res.* **2009**, *682*, 71−81.
(58) Montesano, F. F.; Parente, A.; Santamaria, P.; Sannino, A.; Serio, F. Biodegradable Superabsorbent Hydrogel IncreasesWater Retention Properties of Growing Media and Plant Growth. *Agric. Agric. Sci. Procedia* **2015**, *4*, 451−458.
(59) Wyciszkiewicz, M.; Saeid, A.; Górecki, H.; Chojnacka, K. New generation of phosphate fertilizer from bones, produced by bacteria. *Open Chem.* **2015**, *13*, 951−958.
(60) Pantano, G.; Mazzeo, D. E. C.; Rocha, T. H. S.; Marin-Morales, M. A.; Fadini, P. S.; Mozeto, A. A. Toxicity of the sawdust used for phosphorus recovery in a eutrophic reservoir: experiments with *lactuca sativa* and *allium cepa*. *Environ. Sci. Pollut. Res.* **2021**, *28*, 18276−18283.
(61) Das, S.; Dalei, G. In situ forming dialdehyde xanthan gum-gelatin Schiff-base hydrogels as potent controlled release fertilizers. *Sci. Total Environ.* **2023**, *875*, No. 162660.
(62) Nooeaid, P.; Chuysinuan, P.; Pitakdantham, W.; Aryuwananon, D.; Techasakul, S.; Dechtrirat, D. Eco-Friendly Polyvinyl Alcohol/Polylactic Acid Core/Shell Structured Fibers as Controlled-Release Fertilizers for Sustainable Agriculture. *J. Polym. Environ.* **2021**, *29*, 552−564.
(63) Arruda, A. d. S.; Silva, W. C.; Oliveira, R. C.; Lemes, E. M.; Guimarães, G. S.; Júnior, R. J. O.; Luz, J. M. Q. Cytogenotoxic effects of nitrogen on hydroponic lettuce. *BioscI. J.* **2021**, *36*, 217−227.
(64) Magdaleno, A.; Paz, M.; Weigandt, C.; Iorio, A. F.; Moretton, J. Micronucleus and chromosome aberration frequencies in allium cepa cells exposed to coastal sediments from a polluted estuarine system. *Braz. J. Aquat. Sci. Technol.* **2022**, *25*, 8.
(65) Salah, M.; Yehia, S.; Ali, R. T. Cytogenetic effect of some nanostructure polymers prepared via gamma irradiation on *Vicia faba* plant. *Chem. Biol. Technol. Agric.* **2022**, *9*, No. 6.
(66) Jastrzębska, M.; Kostrzewska, M. K.; Saeid, A.; Jastrzębski, W. P. Do New-Generation Recycled Phosphorus Fertilizers Increase the Content of Potentially Toxic Elements in Soil and Plants? *Minerals* **2021**, *11*, 999.
(67) Arora, K.; Singh, N.; Srivastava, S.; Srivastava, A. Evaluation of Genotoxic Risks Due to Temporal Changes in Soil Urea: Using *Allium cepa* L. Root Tip Bioassay. *Cytologia* **2014**, *79*, 85−93.
(68) Doroftei, E.; Tradafirescu, M. Cytotoxic effects and mutagen potential induced by the foliar fertilizer Bionat on *Allium cepa* L. *J. Environ. Prot. Ecol.* **2013**, *14*, 1627−1636.
(69) Bonciu, E.; Roşculete, E.; Olaru, A. L.; Roşculete, C. A. Evaluation of the mitodepressive effect, chromosomal aberrations and nuclear abnormalities induced by urea fertilization in the meristematic tissues of *Allium cepa* L. *Caryologia* **2018**, *71*, 350−356.

CAS BIOFINDER DISCOVERY PLATFORM™
ELIMINATE DATA SILOS. FIND WHAT YOU NEED, WHEN YOU NEED IT.
A single platform for relevant, high-quality biological and toxicology research
Streamline your R&D
CAS
A division of the American Chemical Society

https://doi.org/10.1021/acsagscitech.4c00243
ACS Agric. Sci. Technol. 2025, 5, 142−157